A Search for $\mu^- N \rightarrow e^- N$ with Sensitivity Below 10^{-16}

M. Bachman, T.J. Liu, W. Molzon*

University of California, Irvine

A. Empl, E.V. Hungerford, K. J. Lan,
B.W. Mayes, L.S. Pinsky, M. Youn

University of Houston

R.M. Djilkibaev, A.K. Skasyrskaya, A.N. Toropin

Institute for Nuclear Research, Moscow

W.D. Wales

University of Pennsylvania

D. Koltick, I. Levine, Y. Pischalnikov

Purdue University

September 1996

Letter of Intent

* Contactperson

Contents

1 Introduction

We intend to propose to search for the process $\mu^- N \rightarrow e^- N$ with a significantly improved sensitivity with respect to past and proposed future searches. This process, if observed, will provide direct evidence of muon and electron number violation. The experiment would be conducted in a new muon beam line at the AGS, produced using a pulsed proton beam. The energy will be chosen in the range 8-20 GeV to optimize the muon flux per unit time and minimize operating costs of the experiment. The expected sensitivity, normalized to the kinematically similar process of muon capture on the nucleus, is one event for a branching fraction below 5×10^{-17}.

In this letter of intent, we briefly review the physics motivation for such a search, discuss the present status and expected results of other experiments with related goals, outline the basic ideas of the experiment, and discuss the status and results of studies of the important experimental issues. We request the help of the laboratory in preparing a full proposal in the next 6-8 months.

1.1 Physics Motivation for LFV Searches

The primary physics goal of this initiative is the study of the conservation of additive quantum numbers associated with each lepton family. Violation of these quantum numbers is commonly referred to as lepton flavor violation (LFV). In this section we give a brief motivation for such experiments.

The motivation is twofold. First, conservation laws associated with each family of leptons are among a restricted list of discrete conservation laws which appear to be exact. Other such laws are those associated with electric charge, total lepton number, and baryon number. There laws are derived from experiment and there is a fundamental experimental interest in testing them. Further, only the conservation of electric charge is well motivated theoretically. Here, the conserved quantity (electric charge) is associated with the local gauge theory of electromagnetic interactions. In the case of baryon number, total lepton number, and numbers associated with each family of leptons, there is no interaction for which invariance under a local gauge transformation predicts a conserved quantity. Hence, there is a strong theoretical prejudice that violations of all these quantum numbers will be observed eventually.

There continues to be intense experimental effort in testing conservation laws; there are ongoing experiments searching for LFV, lepton number violation (neutrinoless double beta decay), and baryon number violation (proton decay and neutron - antineutron oscillations). There are substantial new efforts devoted to many of them.

Aside from the fundamental discovery of the breakdown of a conservation law, the discovery of LFV processes would also demonstrate that the Standard Model of particle interactions is incomplete. This discovery would indicate the existence of a new force (mediated by new gauge bosons), or the existence of a new class of heavy particles. In the first case the reaction would occur through the exchange of a new gauge boson which explicitly couples leptons of different families to each other. In the second case, the process would occur via family mixing in some new sector (e.g. supersymmetry).

In the model of Cahn and Harari [1], LFV decays are classified by the change in a *generation number* with value 1 for the lightest quarks and leptons, 2 for the intermediate mass

fermions, and 3 for the heaviest family of fermions. Kaon decay experiments are sensitive to interactions in which generation number is conserved, while the process $\mu^- N \rightarrow e^- N$ is sensitive to those in which generation number changes by one unit. Table 1 lists various LFV processes, the corresponding change in *generation number*, the present experimental limit, and the corresponding mass limit.

Process	Δ G	limit	mass limit (TeV)
$K_L^0 \rightarrow \mu e$	0,2	2.4×10^{-11}	100
$K^+ \rightarrow \pi \mu e$	0	2.1×10^{-10}	29
$\mu \rightarrow eee$	1	1.0×10^{-12}	86
$\mu \rightarrow e\gamma$	1	1.7×10^{-11}	20
$\mu^- N \rightarrow e^- N$	1	8×10^{-13}	500

Table 1: Process, change in generation number, experimental limits, and inferred limits on intermediate particle masses for different LFV processes.

More interest has occurred recently in the second scenario, where LFV occurs in supersymmetric grand unified theories. These models are particularly attractive, as supersymmetry is perhaps the most realistic candidate to solve many of the shortcomings of the Standard Model. Much of the experimental effort at high energy colliders (LEP, the Tevatron, the LHC) is directed towards discovering new massive particles at about the electroweak symmetry breaking scale, and much of that is devoted to supersymmetry searches. It has recently been realized that LFV will occur at experimentally accessible levels in a large class of supersymmetric models [2, 3, 4, 5]. Further, in some specific grand unified supersymmetric models, the rate for LFV processes can be directly related to standard model parameters. A set of Feynman diagrams from one supersymmetric model is shown in figure 1, taken from reference [5]. The predicted rates for the process $\mu^- N \rightarrow e^- N$ are plotted in figure 2. In the same model, the expected rates for the process $\mu \rightarrow e\gamma$ are shown in figure 3.

A search for $\mu^- N \rightarrow e^- N$ with sensitivity of 10^{-16} represents a tremendous improvement in experimental knowledge and, if grand unified supersymmetric models are correct, has a real chance of a discovery.

1.2 Present Experimental Status of LFV Searches

Despite sensitive experimental searches extending for over 30 years, no evidence for the existence of LFV processes has been observed. In the past ten years there has been significant improvement in the limits on LFV-experiments involving both kaon and muon decays. The present limits are given in table 1.

In kaon decay experiments, there are two ongoing experiments which will improve sensitivity by at least a factor of 10. E871 at BNL has data on tape which could yield a sensitivity for the process $K_L^0 \rightarrow \mu e$ of 1 event for a branching fraction of 10^{-12}. E865, also at BNL, has a proposed sensitivity approaching 10^{-12}. KAMI at Fermilab, if executed, could in principle improve on the neutral K sensitivity by a further substantial factor.

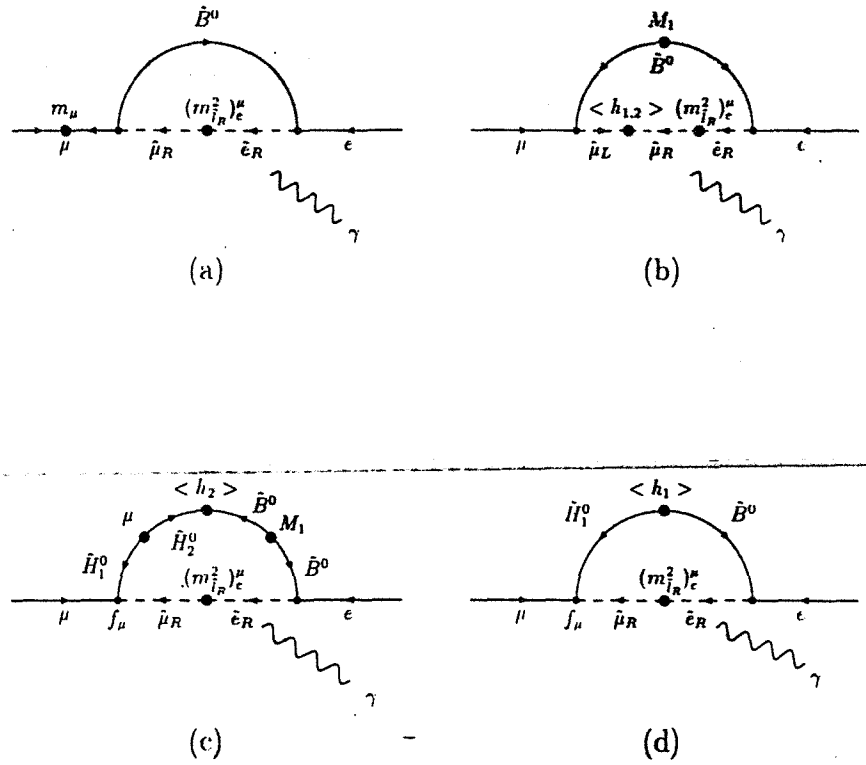

Figure 1: Examples of Feynman diagrams for $\mu^- N \rightarrow e^- N$ containing supersymmetric partners of SM particles. The same diagrams contribute to $\mu \rightarrow e\gamma$.

In muon processes, MEGA at LAMPF has a proposed sensitivity below 10^{-12} for $\mu \rightarrow e\gamma$. They have finished their data taking and have data on tape which should allow a limit near that level. There are no other active proposals to further improve sensitivity, although there exists an idea due to Kuno, Mori and Yokada [6] for improving the $\mu \rightarrow e\gamma$ sensitivity by about a factor of 100. For the process $\mu^- N \rightarrow e^- N$, the best limit is now 8×10^{-13} from the SINDRUM2 collaboration. They are building a new beam which, together with modified analysis techniques, could push that sensitivity to 1 event for a branching fraction of 4×10^{-14}. Djilkibaev and Lobashev [7] proposed a method for achieving a sensitivity of 1 event for a branching fraction of 10^{-16} which resulted in a proposal, MELC [8] to do this experiment at the Moscow Meson Factory. This proposal is now inactive; we discuss it in more detail below since many of the ideas of our proposal are based on it.

We believe the motivation for continuing these experiments remains as strong as ever, assuming significant experimental advances can be made. Where the first evidence for LFV will be found is not predictable, and significant increases in sensitivity in all possible channels are well motivated.

2 Outline of the Experiment

The process of muons converting to electrons in the field of a nucleus may not be familiar to many high energy physicists, and we review the basic idea of the experiment here.

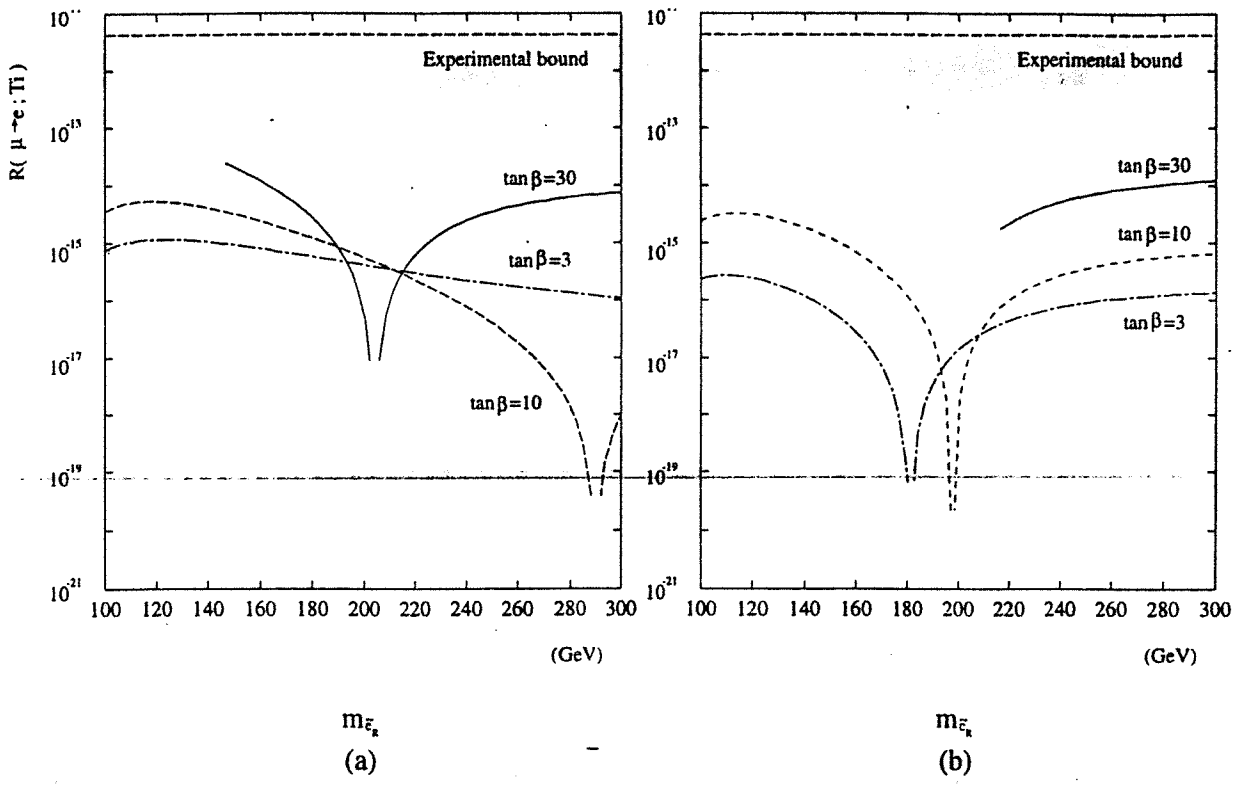

Figure 2: Expected rates for $\mu^- N \rightarrow e^- N$ in the model of Hisano, et al., for different values of the ratio of Higg's particle vacuum expectation values, as a function of the right handed squark mass. The plots are shown for the parameter $\mu > 0$ (a) and $\mu < 0$ (b).

Negative muons, when stopped in matter, quickly cascade down to an inner atomic orbital of size comparable to that of the nucleus. The muons will mostly either decay or be captured on the nucleus: for example $\mu^- Al \rightarrow \nu Mg$. For aluminum, these two processes occur at about the same rate and hence the number of muons remaining decreases with a lifetime of about half that of muons in vacuum, or about 1 μsec. A third possibility is that a muon, in interacting with a nucleus, converts to an electron. The rest energy of the muon is largely converted to kinetic energy of the electron, since the heavy nucleus recoils with momentum equal to the electron momentum and negligible kinetic energy. Hence, the experimental signature is an isolated electron with energy equal to the muon mass less the Coulomb binding energy of the muon in the nucleus, or about 105 MeV.

The momentum transfer to a nucleon within the nucleus is such that the nucleus is left in its ground state. Therefore, the process is coherent over all nucleons and the rate is enhanced by approximately a factor of A. Calculations of the precise level of coherence have been done and the rate for various nuclei predicted [9, 10]. The conversion rate is conventionally normalized to the kinematically similar process $\mu^- N \rightarrow \nu N'$. In both cases, the final state consists of a nucleus and a light lepton with energy equal to nearly the rest energy of the muon. We define the quantity $R_{\mu e} = \Gamma(\mu^- N \rightarrow e^- N)/\Gamma(\mu^- N \rightarrow \nu N')$. For a given LFV process, the expected value of $R_{\mu e}$ increases linearly with Z for low Z and more slowly for large Z. Hence, lacking other considerations, the experiment is best done with

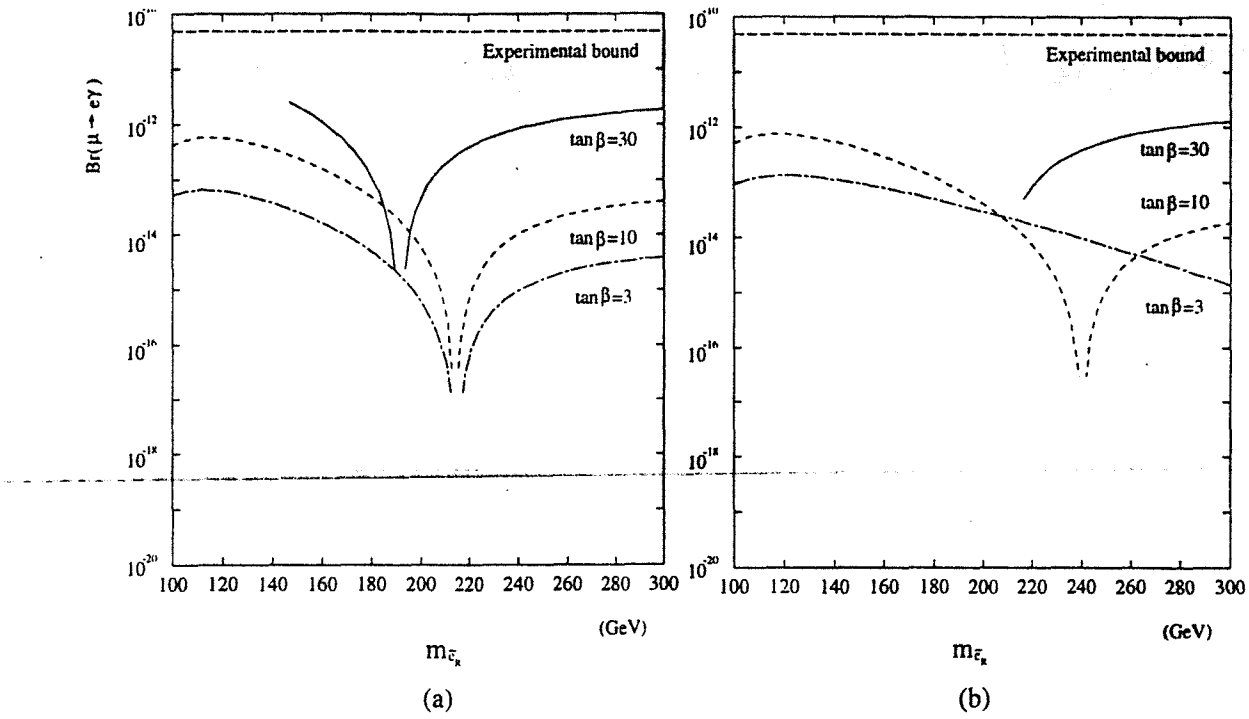

Figure 3: Expected rates for $\mu \rightarrow e\gamma$ in the model of Hisano, et al., for different values of the ratio of Higg's particle vacuum expectation values, as a function of the right handed squark mass. The plots are shown for the parameter $\mu > 0$ (a) and $\mu < 0$ (b).

large nuclei.

If the interaction with the nucleus is mediated by a photon, the process is closely related to the decay $\mu \rightarrow e\gamma$. While there appears to be some confusion about the relative rates at which these two processes occur, the consensus is that the branching fraction for $\mu \rightarrow e\gamma$ would be a factor of 100-200 greater than the probability of conversion of a μ^- in a Coulomb orbit [11]. A typical case is shown in figures 2 and 3. Here, the interference of multiple diagrams produces zeros in the rates for particular model parameters, but typically the ratio of branching fractions is about 100.

In other models, in which the process is mediated by something other than a photon, the branching fraction for $\mu^- N \rightarrow e^- N$ can be greater than that for $\mu \rightarrow e\gamma$. However, even in the case where $R_{\mu e}$ is 100 times less than B($\mu \rightarrow e\gamma$), the substantial experimental advantages of $\mu^- A \rightarrow e^- A$ experiments may allow an improved sensitivity to the underlying physics using this mode.

The essential advantage of the $\mu^- N \rightarrow e^- N$ experiment with respect to $\mu \rightarrow e\gamma$ is that the former has no accidental background, in the sense that the signature is a single particle and background/signal is independent of the rate at which data is collected. Further, the sources of 105 MeV electrons are very much suppressed. This is contrasted with the case of $\mu \rightarrow e\gamma$. There, the essential backgrounds come both from single radiative muon decays, and from accidental coincidences of an electron from one muon decay, and a photon from another. The rate for the latter process grows as the square of the instantaneous intensity,

and eventually is the dominant source of background.

The principle sources of background for $\mu^- N \rightarrow e^- N$ are electrons from muon decay in orbit, where the electron can have energy equal to that from the signal process, radiative pion capture with an asymmetric photon conversion, muon decays in flight resulting in a high energy electron, scattering of electrons in the beam, and cosmic ray produced electrons.

The experiment we propose is performed by producing an intense muon beam which is caused to stop in the *stopping target*. The signature of $\mu^- N \rightarrow e^- N$ is an electron of energy 105 MeV emanating from the stopping target. To reduce background from muon decay in orbit, the electron energy must be measured with high precision. The measurement is limited by dispersion in the energy loss of the electron as it exits the stopping target and by the resolution of the spectrometer used to measure the energy. Reducing backgrounds below 10^{-16} requires energy resolution (FWHM) below 1 MeV. Other sources of background cannot be eliminated by improved energy resolution and eliminating them requires a pulsed beam, with the conversion electrons detected only a few hundred ns after the pulse of muons is caused to impinge on the stopping target. To achieve the desired sensitivity, the experiment must operate in a high flux of charged particles, neutrons, and photons, putting severe constraints on the detector.

3 Current Status of $\mu^- N \rightarrow e^- N$ Experiments

The current best limit for $\mu^- N \rightarrow e^- N$ derives from the SINDRUM2 experiment at PSI, which has set an upper bound [12] $R_{\mu e} < 8 \times 10^{-13}$ (90% CL), as yet unpublished. Previous best limits derived from experiments at TRIUMF [13] and at PSI [14].

The SINDRUM2 collaborations proposes to improve their sensitivity to 4×10^{-14} with a new beam and new background rejection technique. It is instructive to look at the SINDRUM2 experiment to understand why the technique used there cannot be pushed significantly farther and to motivate what changes must be made to get substantial improvement. Figure 4 shows a cut view of the SINDRUM2 apparatus. It is a cylindrical detector in a solenoidal field, with drift chambers to measure the electron momentum. The beam is a mix of muons, pions and electrons and is essentially continuous. Muons are stopped in a target on the axis of the solenoid at a rate of about $10^7 s^{-1}$.

The electron energy resolution in the SINDRUM2 case is limited by dispersion in the energy loss as electrons exit the target and traverse scintillation counters in the detector; the FWHM is about 2 MeV. That resolution is sufficient to eliminate the muon decay in orbit background at the sensitivity achieved. Backgrounds from radiative pion capture, scattered electrons, and muon decay in flight are eliminated by rejecting events in which there is a signal in a thin scintillator in the beam, time coincident with the detected electron signal.

Figure 5 shows the energy spectrum of electrons before two sets of cuts are applied. The first set is designed to eliminate cosmic ray induced backgrounds, and basically consists of removing events with other signals in the detector. The background removed by these cuts is shown as the heavy shaded area. The lighter shaded area are those events eliminated by requiring no time coincident signal in the beam scintillator. The lightest shading indicates the events remaining after all cuts, which are presumably dominated by muon decay in orbit. The expected signal (shown as dots) is sufficiently separated in energy from this background.

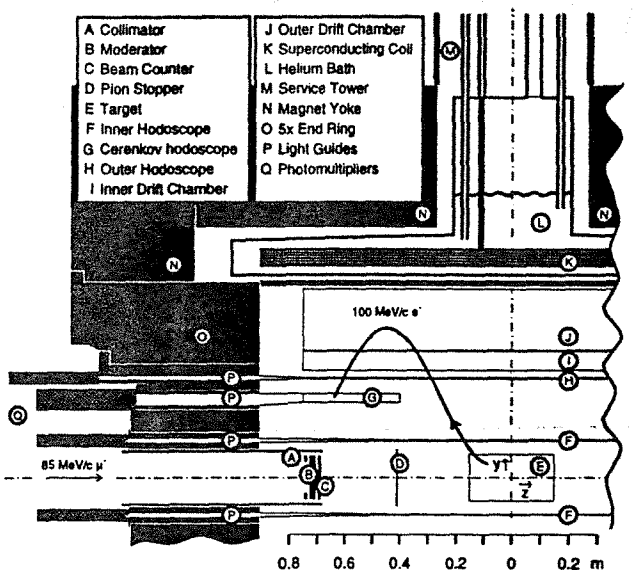

Figure 4: A cut view of the SINDRUM2 $\mu^- N \rightarrow e^- N$ apparatus.

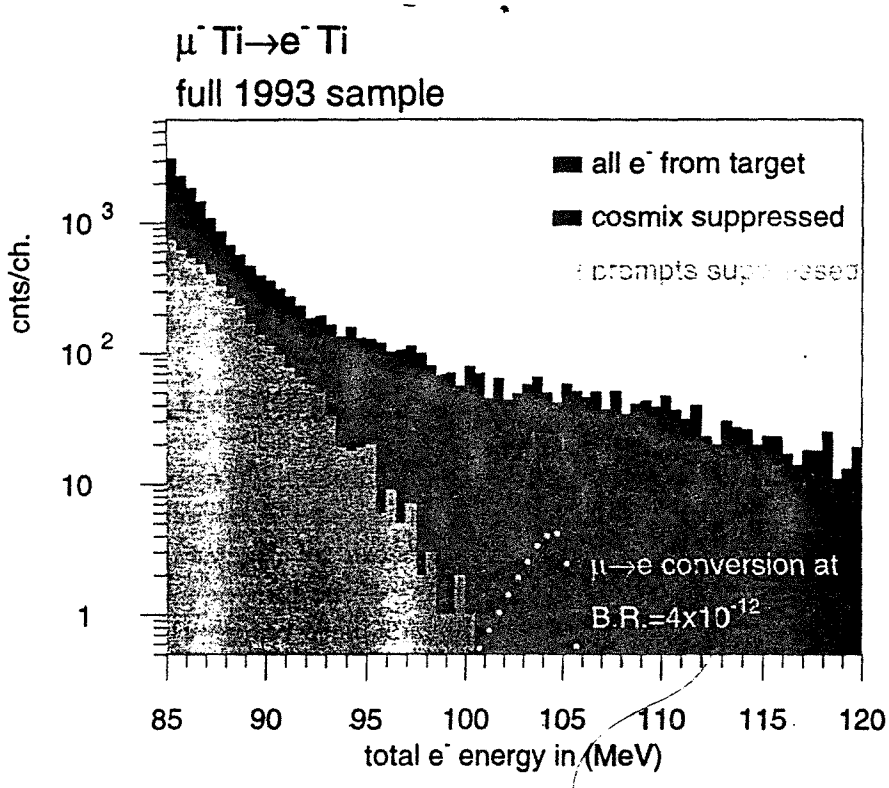

;ure 5: Histogram of the electron energy distribution from the SINDRUM2 experiment. e unshaded is after all cuts, lightly shaded are events removed by "prompt" cuts, and the ıvily shaded is events removed by cosmic ray cuts.

To further improve their sensitivity, the SINDRUM2 collaboration proposes to increase the stopping rate to $10^8 s^{-1}$, at which point they will no longer be able to use a beam veto. They propose to eliminate the prompt background by purifying the beam, eliminating all pions, and reducing the beam energy so that muons decaying in flight will not result in electrons sufficiently energetic to cause backgrounds. The beam they propose to use is shown in figure 6. It uses an absorber on the axis of a solenoid to absorb undecayed pions. From

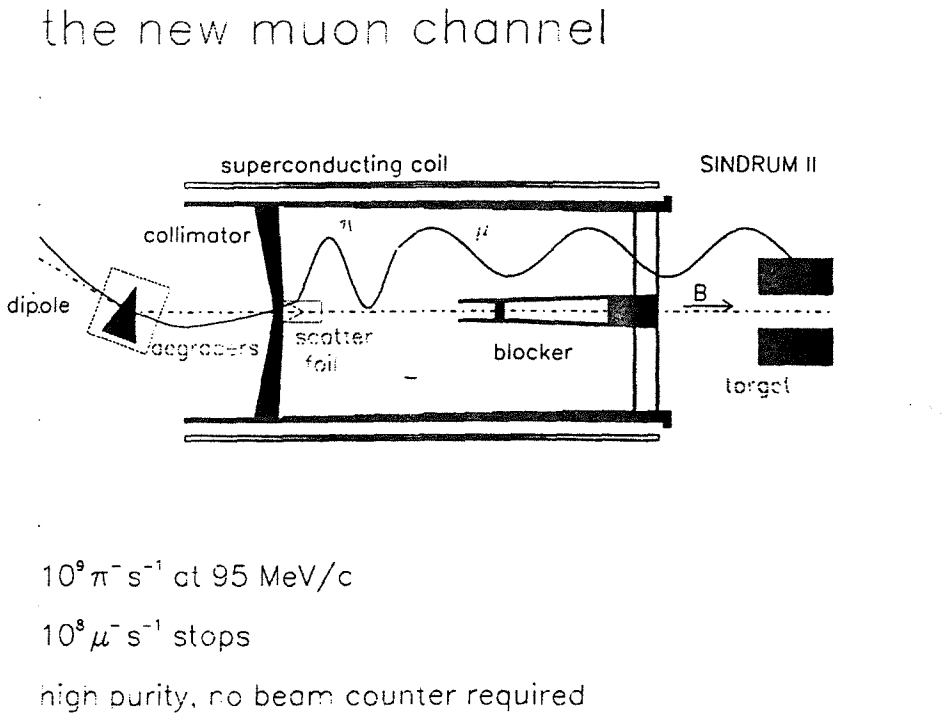

Figure 6: A cut view of the new SINDRUM2 muon beam .

figure 5, we see that the prompt veto eliminates about 200 events in a sample with a limit of 8×10^{-13}, implying about 4000 events of that type for a sample which would yield a limit of 4×10^{-14}. Hence, the beam will have to be cleaner by a factor of 4000 to be background free. Improving the sensitivity by a further 3 orders of magnitude using similar techniques sounds implausible. It is this consideration which leads us to believe that a pulsed beam is required, such that there are no particles in the beam during the time that the conversion electrons are detected. Proponents of the MELC experiment had reached the same conclusion without benefit of the SINDRUM2 experience.

Cosmic ray background in the SINDRUM2 detector is thought to come primarily from photon conversions in the stopping target. They eliminate events with extra track segments in the detector. We note that cosmic ray background is proportional to running time, not the sensitivity. Hence, an experiment running for similar time and with similar cosmic ray vetoing probability should be cosmic ray background free.

From figure 5, we see that the intrinsic background due to muon decay in the Coulomb

bound orbit is well separated from the signal region. To improve the sensitivity by 10000 with respect to this experiment, the electron resolution must be improved substantially. Near the endpoint, the background is proportional to $(E_{max} - E)^5$[15]. Hence, the SINDRUM2 collaboration, with their resolution, should expect about 1 background event per MeV at 102.5 MeV (a factor of 2 closer to the endpoint than the present 1 background event level) with about 32 times the sensitivity, or about the expected new SINDRUM2 sensitivity. At substantially lower sensitivity, this background will swamp the signal unless significant improvement in the resolution is achieved.

4 The MELC Proposal

Many of the ideas for the experiment we intend to propose are based on the ideas of Lobashev and Djilkibaev [7] which resulted in the MELC proposal [8] to do this experiment at the planned Moscow Meson Factory. It now appears as if it will not be possible to do the experiment there. Figure 7 shows the original conception of the MELC muon beam and

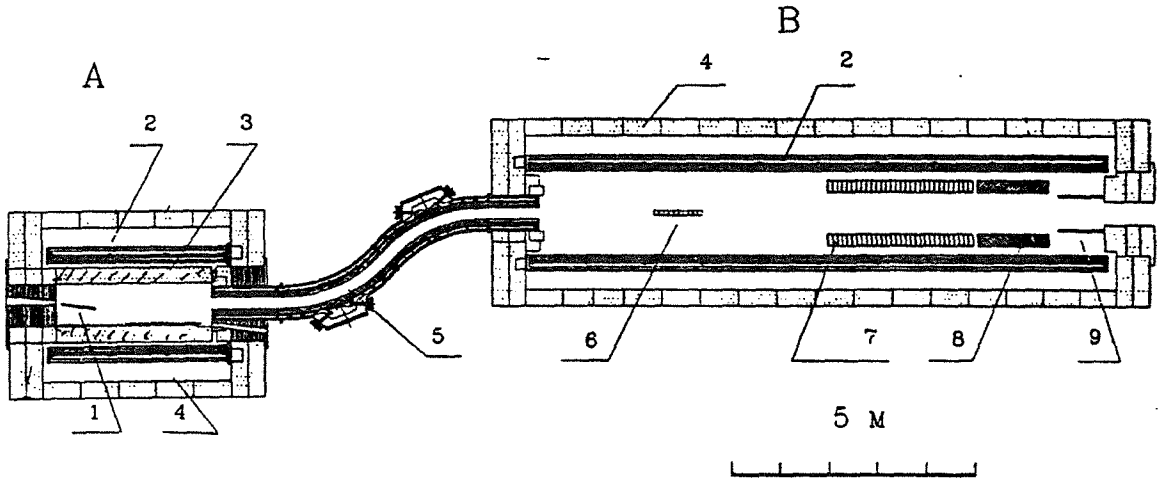

Figure 7: A drawing of the originally proposed MELC apparatus. The essential elements are 1) the proton target, A2) the production solenoid, 5) the transport solenoid, 6) the muon stopping target, B2) the detector solenoid, 7) the tracking detectors, 8) the electron identifying detectors, and 9) the dump. The proton beam enters the production solenoid through a port just below the muon beam exit port.

apparatus.

Briefly, the experiment is done by producing a pulsed beam of a few times 10^{11} low energy negative muons per second and causing them to impinge on a thin target in which a substantial fraction of the beam stops. They are produced by causing protons to impinge on a production target in a high field solenoid; a large fraction of the produced pions decay with the resulting muons being captured in the system of solenoids and transported to the stopping target. The beam pulses are short compared to τ_μ and separated by a time

comparable to τ_μ. An aluminum stopping target is chosen so that the rate at which muons disappear (either through capture or decay) is of order 1 μs. This allows conversion electrons to be detected in a 500 ns window about 500 ns after the muon pulse. Detectors are arranged so that only electrons above 53 MeV pass through them and are measured.

The energy of conversion electrons is measured with a precision of about $\sigma_{RMS} = 0.5\ MeV$ in a magnetic spectrometer with solenoidal geometry. The detector is separated from the target along the axis of the solenoid so that the solid angle subtended by the detectors is reduced, minimizing rates in the detectors from photons originating in the stopping target.

This proposal is now inactive. The collaboration proceeded rather far in the design and construction of the solenoids. They have available the superconducting cable to make the magnets, and also a quantity of aluminum of the appropriate type to make the cryostats. In addition they have the high quality steel needed for magnet return yokes and field shaping pieces.

We have taken a number of essential features of our experiment from the MELC proposal. First, the idea of the pulsed beam is essential to eliminate some backgrounds. Second, the important features of the muon beam, including the production target in a solenoid and solenoid transport of the muons to the stopping target is essential to get the requisite flux. Our most likely detector design also uses the idea of a stopping target displaced along the axis from the detector elements, and uses the MELC idea of placing the target in a region of the solenoid in which the axial field is linearly decreasing in the direction towards the detector.

More detail on the sources of background and a discussion of the ideas for the beam and apparatus are discussed in subsequent sections.

5 Physics Background Sources

The backgrounds to the $\mu^- N \rightarrow e^- N$ experiment motivate many of the basic ideas of our experiment. The primary sources are:

1. Muon decay in a Coulomb bound orbit, with an electron energy endpoint at the same energy as the signal.

2. Radiative muon capture on a nucleus; for an aluminum target the maximum photon energy is 102.5 MeV.

3. Radiative pion capture on a nucleus, with a photon energy up to the pion mass, followed by asymmetric conversion in the stopping target.

4. Muon decay in flight.

5. Beam electrons which scatter in the stopping target.

6. Cosmic ray induced electrons

The first 2 sources cannot be eliminated and can only be minimized by improving the measurement of the electron energy. The first is dominant and the cross section is approximately proportional to $(E_{max} - E_e)^5$ near the endpoint [15]. Hence the signal/background

ratio is extremely sensitive to resolution. Figure 8 shows the signal and background for various values of $R_{\mu e}$ for a resolution of $\sigma_E \simeq 0.5\ MeV$ as simulated by the MELC collaboration. The signal for a value of $R_{\mu e}$ of 10^{-16} is only marginally convincing at the level of a few detected events. We believe a resolution approaching 250 keV is necessary to make a

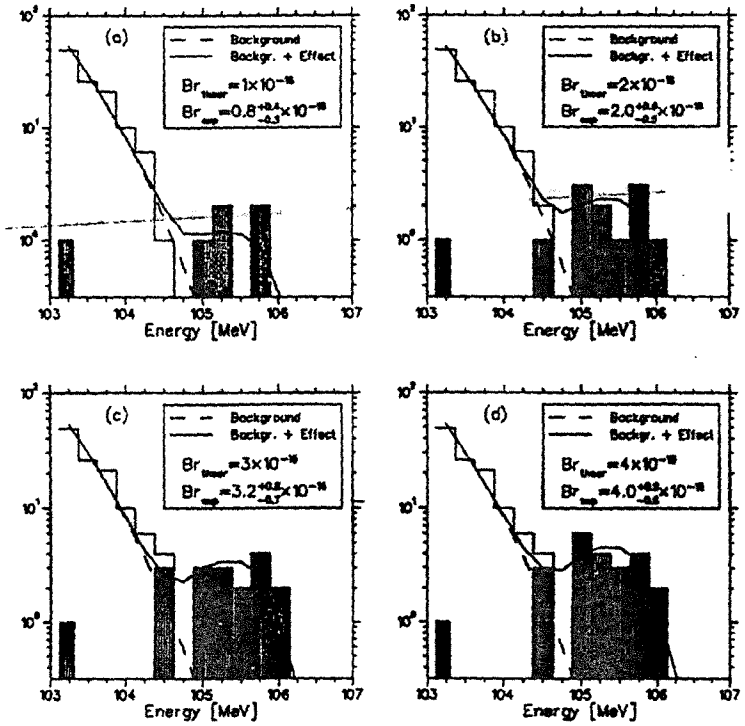

Figure 8: A simulation from the MELC collaboration of the expected signal and background for various values of $R_{\mu e}$ for the tracking chamber thickness equal to 10 mg. per plane.

convincing case at the 10^{-16} level with a small number of events. We discuss in subsequent sections the design of a detector with resolution approaching what we believe is necessary to do this experiment. In the MELC proposal [8], radiative muon capture was shown to be below 10^{-17} and the level of suppression of this background is not affected by the differences between our proposal that one.

Background sources 3-5 derive from prompt processes, with the electron detected close in time to the arrival of a beam particle in the detector. The SINDRUM2 approach to this background was discussed above and clearly does not work at a sensitivity of 10^{-16}. The conclusion arrived at in the MELC proposal, with which we concur, is that a pulsed beam is necessary, in which the probability of particles arriving at the stopping target during the time that conversion electrons are detected is below 10^{-9}. A second method of deriving the required extinction is by reference to the SINDRUM2 data. Without their beam veto, they have approximately 200 events in the signal region, at a sensitivity of 1 event for a branching fraction of about 3×10^{-13} or one event at a branching fraction of 10^{-10}. Assuming this is all due to pion contamination in their beam, to get an expected background below .01 events at a branching fraction of 10^{-16} would require a beam extinction of 10^{-8}. The same

scaling of the SINDRUM2 background levels can be applied to the other sources of prompt background.

The MELC proponents have done a ground up estimate of the required extinction and concluded a value of 10^{-9} is required to get a background level at about 10^{-17}. We have only begun detailed beam simulations, which are necessary to calculate the background for our experiment. Preliminary results are discussed in subsequent sections; our conclusion is not very different from that of MELC. A careful estimate of these backgrounds will be important in designing the beam.

We have not explicitly studied the potential cosmic ray background and estimated the level with different shielding schemes. We have noted that the essentially self shielding nature of the SINDRUM2 experiment cannot be used, since the probable source of cosmic ray background is photon conversion in the stopping target, which in our case is not surrounded by an active detector in which the source of photons would be detected. We presume that we will have to have substantial passive shielding of the apparatus, and that active shielding will be needed at least around the stopping target and tracking detector. We again note that the required level of CR background rejection **does not** scale with the sensitivity, but with the running time. Hence, CR rejection at the same level as in SINDRUM2 will suffice.

6 Sources of Detector Rates

Sources of rates in the detectors can be divided into a number of categories.

First, there are mechanisms giving rates during the muon pulse. These are particle decays in flight, scattering of beam particles, secondaries from pion capture in the target, albedo from the beam dump, and possible photons, neutrons, protons, and other particles coming directly from the muon production target. We have not yet done careful estimates of these rates, and make some general comments. First, the beam design should not allow line of sight trajectories from the production target region to the detectors. Similarly, the transport should minimize the probability of high energy protons arriving in the detector region. Second, if there are excessive rates during the stopping pulse, it should be possible to decrease the gain of the detectors during the "flash" so as to minimize radiation damage and sagging of detector gains due to large current draw. Third, the beam dump should be designed in such a way as to minimize albedo. For example, line of sight trajectories can be eliminated by providing a curved exit solenoid to transport the beam to the dump (or another experiment).

Second, there are substantial fluxes of photons, neutrons, and protons from muons stopped in the target. Electrons from muon decay in orbit, and photons, neutrons, and protons from nuclear deexcitation following muon capture are the most copiously produced secondaries. The electrons from muon decay in orbit are mostly below 53 MeV; figure 9 shows the distribution of electron energy for decays of muons bound in magnesium from reference [16]. The detector must be designed to not intercept the majority of these electrons. There are approximately 2 photons per muon capture, with energies of order 10 MeV, and about 0.01 neutrons and protons per capture. The latter are low energy (up to about 20 MeV) but high momentum since they are nonrelativistic. We have estimated the detector rates due to muon decay in orbit and the products of muon capture. They are discussed in

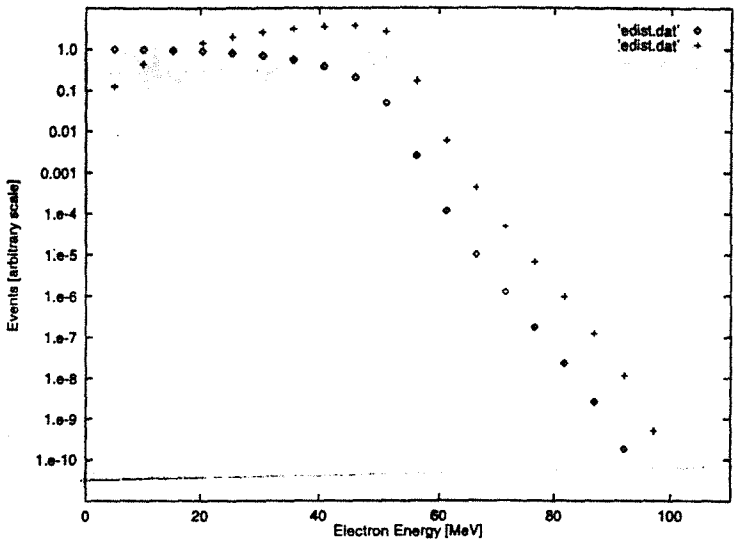

Figure 9: The full energy distribution for muon decay in orbit in magnesium. Shown are the differential probability (+) and the integral probability ($\diamond$) above the energy at which the probability is plotted. About 0.3% of all decay in orbit electrons are above 55 MeV.

the section on the proposed detector.

Clearly, learning from the experience of the SINDRUM2 experiment, even though we would need to extrapolate by 10^4, would be valuable. We have requested from them the value of rates in their detector and have not yet received a reply.

7 Choice of Accelerator for the Experiment

Experiments using low energy muon beams have until now been done at low energy machines (PSI, LAMPF, TRIUMF). Typically, the ratio of usable produced muons to targeted protons was of order 10^{-8}. For the MELC experiment, Djilkibaev and Lobashev proposed to put the pion production target in a solenoidal field and collect pions over essentially 4π solid angle. They calculated it should be possible to produce significantly more muons per proton (10^{-4}) with such a scheme. Coupled with the very high currents possible at these machines, significant improvements in sensitivity could be contemplated. The Moscow Meson Factory, for which MELC was proposed, will not be able to operate enough to execute a sensitive experiment. The TRIUMF cyclotron could plausibly accelerate sufficient protons to produce the necessary muon flux; for scheduling and financial reasons we cannot foresee doing the experiment there in the near future. PSI has a planned program to reach below 10^{-13}, but further increases in sensitivity do not seem possible, again because the required beam conditions cannot be met.

Recently, it has been realized, perhaps first by the muon collider proponents, that a significantly larger ratio of usable muons to targeted protons can be achieved at BNL. The achievable flux is discussed below. Although somewhat uncertain, it is in the required range. Further, it appears as if the requisite pulsed beam could be produced.

Another possibility, which we have not explored extensively, is to use the Fermilab

booster. It appears difficult to get a pulsed beam from that machine and the operating conditions would probably not be consistent with other running.

8 Pulsed Proton Beam

We have begun a study of the intensity and time structure of a beam which could be made at BNL. The energy at which the machine would be run is a compromise between producing the maximum muon flux and minimizing the operating costs. By running at lower energy, the cycle time would be less, the running cost would be less, and the machine would be easier to run if it was below transition. On the other hand, the pion production cross section is down. We have not fully explored that optimization, but it appears likely that we would run at 8 GeV, with a macro duty factor of 50% (one second spill with two second cycle time). We would probably want the maximum intensity which could be achieved.

We have explored a number of ways in which the BNL proton beam can be pulsed. Recall the pulsing is intended to produce short (much less than τ_μ) pulses of muons separated by approximately τ_μ. Two possibilities exist using the AGS.

The first is to use the RF structure of the beam, and extract it bunched. The AGS RF has 8 bunches in the 2.7 μs revolution time. Hence, filling only two bunches would give a pulse spacing of 1.35 μ. Space charge effects limit the intensity per bunch to $1 - 2 \times 10^{13}$ protons which may limit the delivered intensity in this extraction scheme.

With the help of AGS personnel, we have made a first set of measurements of the quality of such a pulsed beam. One RF bunch was filled, accelerated to 24 GeV, and extracted without debunching. An RF signal synchronized with the pulse was supplied to the E871 experiment, and we measured the rate of E871 triggers at various times with respect to the RF bunch. The E871 trigger is a six-fold scintillator coincidence, and is mostly satisfied by decays of kaons made in the production target. Hence, its rate is strongly correlated with the rate of protons hitting the target. For 10^7 counts in a 50 ns window around the filled RF bunch, we counted about 10 triggers (depending on beam conditions) in a 200 ns gate between RF bunches, and about 10^4 counts in a nominally unfilled bunch. Hence, the extinction between bunches is about 10^{-6} and in unfilled bunches is of order 10^{-3}. The precise shape of the extracted pulse was measured by another experiment, and those results are not yet available.

A second way to extract a bunched beam is to use barrier RF buckets. With an unbunched beam, two empty RF buckets are produced adjacent to each other and then separated in phase, resulting in an empty region in the ring. The beam is extracted by exciting a resonance which pushes beam between the RF buckets, and then to extraction. In principle, beam is only extracted in this narrow phase in the ring. Multiple pairs of barrier buckets could be inserted in the ring if we wanted a pulse frequency of any integral multiple of the revolution frequency of the machine. Barrier bucket extraction has been tested at a much higher frequency (100 MHz) with pulse widths of about 400 ps. We plan to test this means of extraction at a frequency appropriate to our use in the FY96 AGS run.

8.1 Secondary extinction devices

It appears likely that it will not be possible to reach an extinction below 10^{-8} in the extracted beam, and we are exploring other means of reducing the off pulse rate. One possibility is to use a fast kicker magnet running at the pulse frequency to divert the beam from the production target between pulses. Kicker magnets with rise times of tens of ns have been made, but have not been run at this frequency. We have discussed with a number of Fermilab personnel possibilities for running these magnets at high frequency, and it seems promising. For example, a 0.01 T magnet 4 m long with 5 by 10 cm^2 bore and a ferrite flux return pulsed at 1 MHz deflects a proton beam by 2 cm in a 10 m path and requires 1 MW of pulsed power delivered to the magnet.

Another possibility is to turn off the muon transport between pulses. In some respects this is easier, since the momenta are low, and hence less field is required. The muons are transported in a solenoidal field, and reducing to zero the field in one segment of the solenoid will substantially reduce the transport efficiency. We have have not yet pursued a way of modulating the solenoid field at the required 1 MHz rate.

A third possibility to be considered is that, if the extinction is only 10^{-6} or so, a veto counter active only during the measurement time could be used to further reduce background. There are several problems with this, including radiation damage, high rates from electrons from muon decay in the stopping target, albedo from the beam dump, etc., which must be studied. It appears as if the rates from electrons resulting from muon decay which are not reflected in the detector solenoid make this option unlikely to succeed, but we will continue to pursue it.

9 Muon Beam Design

The muon beam is required to have sufficient intensity to reach the desired sensitivity, to have the appropriate time structure, and to have sufficiently small pion and electron contamination such that they are not a source of physics backgrounds. It is desirable that contamination by positive muons be small and that the flux of high energy muons which do not stop in the detector solenoid be minimized, so as to reduce detector rates.

The basic concept of the production scheme was proposed by the MELC collaboration [8] and subsequently by the muon collider[17] proponents. The MELC muon source is shown in figure 7; it consists of a production target in a high field solenoid, with a lower field solenoid matched to the exit to transport muons to the stopping target. We have begun a study of the optimization of a production and transport scheme with similar design. The flux depends on the pion production cross section at low pion momentum, the target material, and the magnetic field configuration in the production and transport solenoids. Further, the number of muons stopping in the stopping target is of essential concern. Restrictions on the thickness and transverse dimensions of the stopping target arise from background considerations. Hence, the energy spectrum of the produced muons and the transverse size of the muon beam is important. It should have a large flux below 50 MeV/c to maximize stopping, and should intercept a target of radius approximately 7.0 cm.

9.1 Pion Production and Capture

The basic idea of the MELC scheme, which we propose to exploit, is to target an intense proton beam on a high Z target approximately on the axis of a solenoid. The backwards direction (with respect to the muon beam) is arranged to have higher axial field value, forming a magnetic mirror and hence increasing the pion capture probability. Pions with a transverse momentum below some value (which depends on the B field value and the radius of the solenoid) will be trapped and drift along the field lines, ultimately decaying. The resulting muons are transported in a solenoid field to the detector region. Because we are primarily interested in low energy pions, there is probably only a small dependence of the yield on the direction of the incident proton beam.

There exists little data on low energy pion production cross sections in the region of interest, including backwards production. This issue is crucial to the muon collider project, and they have studied it extensively. There now exists an experiment (BNL E910) which has taken data to measure these cross sections. They have shown preliminary results of forward production, which as yet is not corrected for detection efficiency. They also have taken data with the interaction point inside a TPC, from which they should be able to get cross sections over all relevant regions of phase space.

Lacking measurements, we have relied on a number of models of pion production to estimate fluxes. Figure 10 shows the production cross section as a function of kinetic energy, longitudinal momentum and transverse momentum for GHEISHA [18], FLUKA [19], and SHIELD [20]. FLUKA has a significantly different kinetic energy distribution, especially at small kinetic energy. They all agree reasonably well with data in the regions where there is data for comparison.

For a particular choice of muon beam parameters and for 8 GeV protons, the relative yield of stopping muons for GHEISHA:SHIELD:FLUKA is 1.93:1.00:0.38. The numbers are contained in table 2 below. In the rest of the discussion on muon yields, we have used the SHIELD code.

9.2 Solenoid Field Optimization

The design of the production solenoid is intended to optimize the flux of muons which will stop in the stopping target while minimizing other beam particles and minimizing cost. The parameters to be varied are the length and diameter of the solenoid, the magnetic field as a function of axial coordinate, the orientation and position of the target, and the direction in which the proton beam is incident. To maximize the muon yield, pions should be constrained to be near the axis, such that the decay muons have helical centers near the axis and hence will intercept the stopping target. The length should be such that a large fraction of the pions decay in the production solenoid. It is desirable to reflect pions which have initial trajectories opposite in direction to that of the muon beam so that their decay muons will also contribute to the flux.

In these studies, a 24 cm long and 1.2 cm diameter copper or mercury target oriented at 10° with respect to the solenoid axis was used. It is presumed that a relatively thick radiation and heat shield inside the production solenoid will be necessary, which will affect the required solenoid bore. The inner bore of the vacuum space was taken to have a radius of

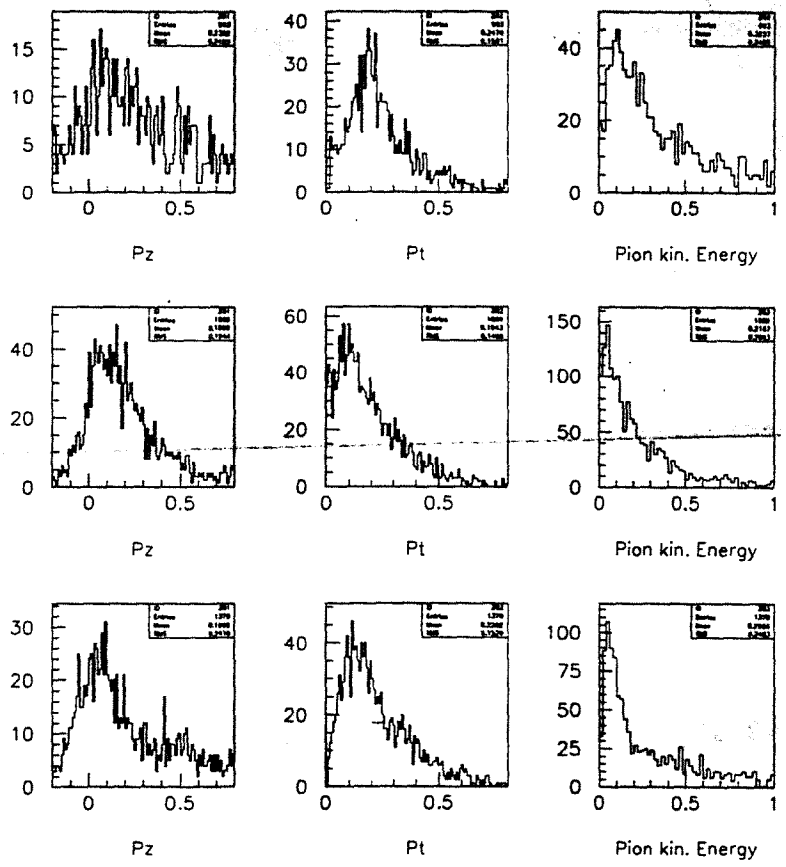

Figure 10: Pion production cross sections as a function of kinetic energy, transverse momentum, and longitudinal momentum for 8 GeV protons incident on copper for FLUKA (top), GHEISHA (middle) and SHIELD (bottom). The vertical scale is arbitrary, but normalized to the same incident proton flux.

30 cm. The beam collimator in the transport solenoid was taken to have a radius of 15 cm. The proton beam was incident opposite to the direction of the muon beam. This direction was chosen to make the construction of the proton exit channel easy (since the target is near the upstream end of the solenoid) and make the radiation and heat shielding of the solenoid easier (since forward going high energy secondaries will mostly go out the proton exit channel). Results are given for 8 and 14 GeV proton energy.

The simulation was done with the GEANT code, using the SHIELD model for pion production. A sketch of the apertures in the solenoid is given in figure 11. Plots of the z (axial) dependence of the axial field component of the five field-configurations studied are shown in figure 12.

The figure of merit for the muon beam is the number of muons stopping in the stopping target. For this study, the target consisted of 25 elements with radius 7.0 cm radius and total thickness of 0.5 cm of aluminum. Table 2 shows the resulting flux of muons, pions, and electrons for the five configurations and two choices of the proton energy and the stopping

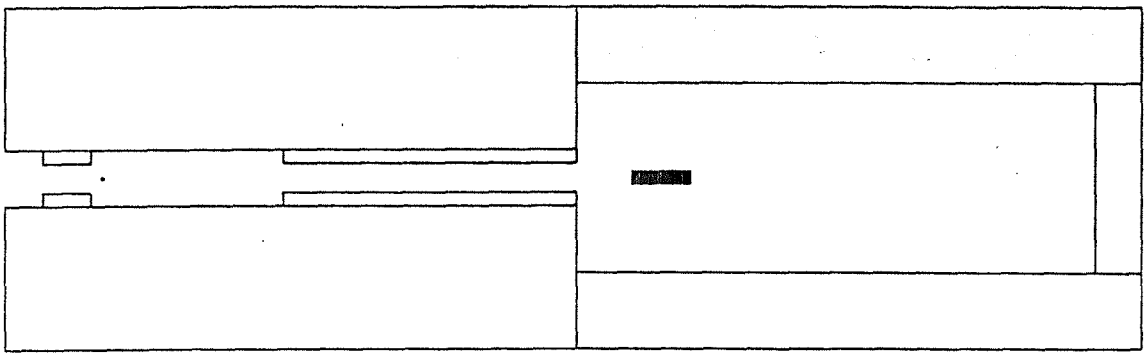

Figure 11: A schematic drawing of the production target and solenoid, transport solenoid, and detector solenoid and stopping target as used in the GEANT calculation of the stopping muon yield.

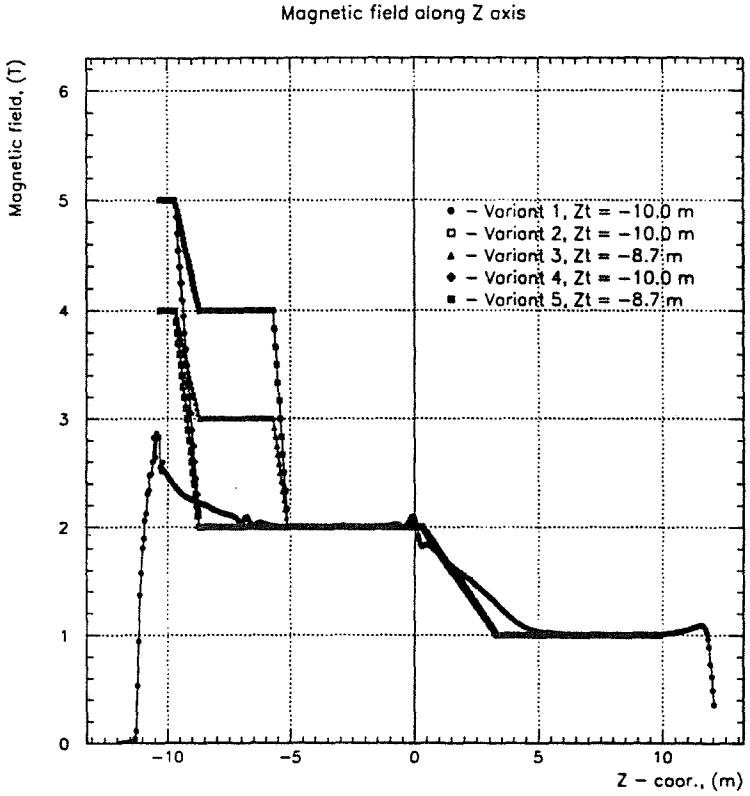

Figure 12: The axial component of the magnetic field as a function of position along the solenoid for the field configurations studied.

rates in the target. Configuration 3, with a maximum field of 4T and a region of 3 m of 3 T field, was taken as a reasonable tradeoff of yield vs cost, and we show various beam properties for this choice. We note that the one calculation with a mercury target is very promising in terms of the muon flux. Clearly, there are technical problems with liquid targets. On the other hand, there are substantial technical problems with cooling any target, and both the muon collider group and spallation neutron groups have discussed the use of heavy liquid

targets. In all our studies we have neglected the problem of target cooling and the affect of the mounting system on the muon yield. We can undoubtedly improve the muon yield, and these studies continue. Figure 13 shows the momentum and kinetic energy distribution of all muons which enter the detector solenoid and those which stop in the stopping target.

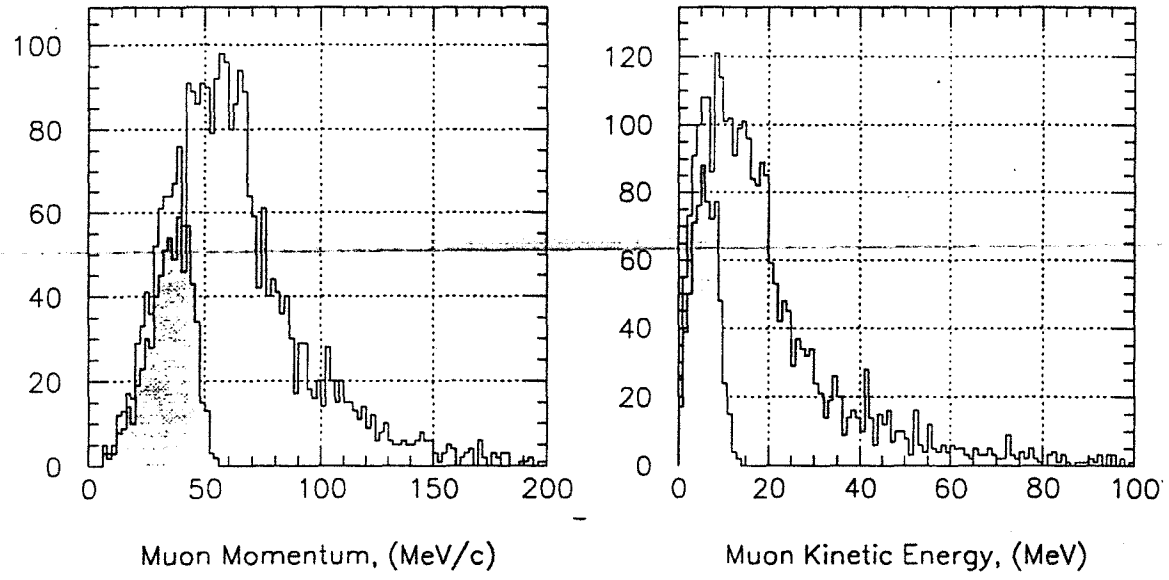

Figure 13: The muon beam momentum and kinetic energy distribution. The full curve is for all muons entering the detector solenoid and the shaded region is for those which stop in the stopping target

We make a few comments on other aspects of the solenoid. The upstream polepiece (near the proton exit channel) must be carefully designed to minimize the production of electrons which will get into the muon beam. This design optimization has not been done. We will also optimize the size of the inner bore of the solenoid, which will depend on the amount of shielding required.

9.3 Mechanisms for purifying the muon beam

Various schemes have been considered for further cleaning the muon beam.

One possibility is curving the transport solenoid. Due to the inhomogeneous nature of the magnetic field, particles are dispersed perpendicular to the bend plane by charge and momentum. The drift distance (motion of the center of the helical trajectory) is given by $D = 1./(0.3B) \times s/R \times (p_s^2 + \frac{1}{2}p_T^2)/p_s$, where s is the path length along the axis of the solenoid, R is the radius of curvature of the solenoid, and p_T (p_s) are the momentum perpendicular and parallel to the axis of the solenoid, respectively. Figure 14 shows the drift distance vs. momentum for muons and pions for a value of s/R of $\pi/2$ (corresponding to a 90° curve in the transport solenoid. Particles can be essentially completely separated by charge, and substantially momentum dispersed. It should be possible to highly attenuate positive particles and high momentum particles which will not stop. By bending in the

Pion Prod Model	Config.	Target	Proton Energy	Total μ	Stop μ	Total π	Stop π	Total e	Stop e
FLUKA	3	Cu	8.	1068	192	324	2	48	1
GHEISHA	3	Cu	8.	2658	950	197	7	267	8
SHIELD	3	Cu	8.	2034	492	227	2	280	10
SHIELD	1	Cu	8.	1431	377	135	1	87	4
SHIELD	1	Cu	14.	1946	487	210	1	118	3
SHIELD	2	Cu	8.	2304	425	298	1	132	2
SHIELD	2	Cu	14.	3075	546	419	4	156	4
SHIELD	3	Cu	8.	2034	492	227	2	280	10
SHIELD	3	Hg	8.	4218	1074	398	6	428	7
SHIELD	3	Cu	14.	2727	624	328	5	400	10
SHIELD	4	Cu	8.	2848	450	400	9	122	2
SHIELD	4	Cu	14.	3789	589	544	4	180	3
SHIELD	5	Cu	8.	2700	495	378	3	359	7
SHIELD	5	Cu	14.	3704	641	475	5	500	14

Table 2: Muon yields for various choices of beam energy, production solenoid configuration, target material and and pion production model, normalized to 10^5 incident protons. The different codes generally agree within about a factor of 2 for the same conditions. The yield goes up with increased production solenoid field, with size of target nucleus, and with the incident proton energy. There is a much higher yield for mercury.

opposite direction after the collimator, the remaining beam can be brought back to the axis of the solenoid.

A second possibility for absorbing pions is to place an absorber on the axis of the transport solenoid. Since pions are produced nearly on the axis, they return to the axis. Muons in general do not, since they are produced at some point along the pion trajectory, in general not on the solenoid axis. We have not yet done a detailed study of this option.

9.4 Beam Time Structure and Backgrounds

A serious concern is physics background from pions stopping during the detection time and radiatively capturing with the photon converting in the target and giving an electron of 105 MeV energy. Such stopping pions can originate from two sources: pions produced by protons which hit the production target during the detection time, and pions produced at the correct time, but which take a very long time to travel from the production target to the stopping target.

We made an estimate of the background level of the first source using the SINDRUM2 observation of prompt backgrounds and that implied an extinction of 10^{-8} would be sufficient for their beam channel. With our simulation, we can estimate the extinction required for our muon beam. From table 2 we see that for configuration 3, the ratio of pion stops to muon stops is about 4×10^{-3}, with large statistical uncertainty. The radiative capture branching

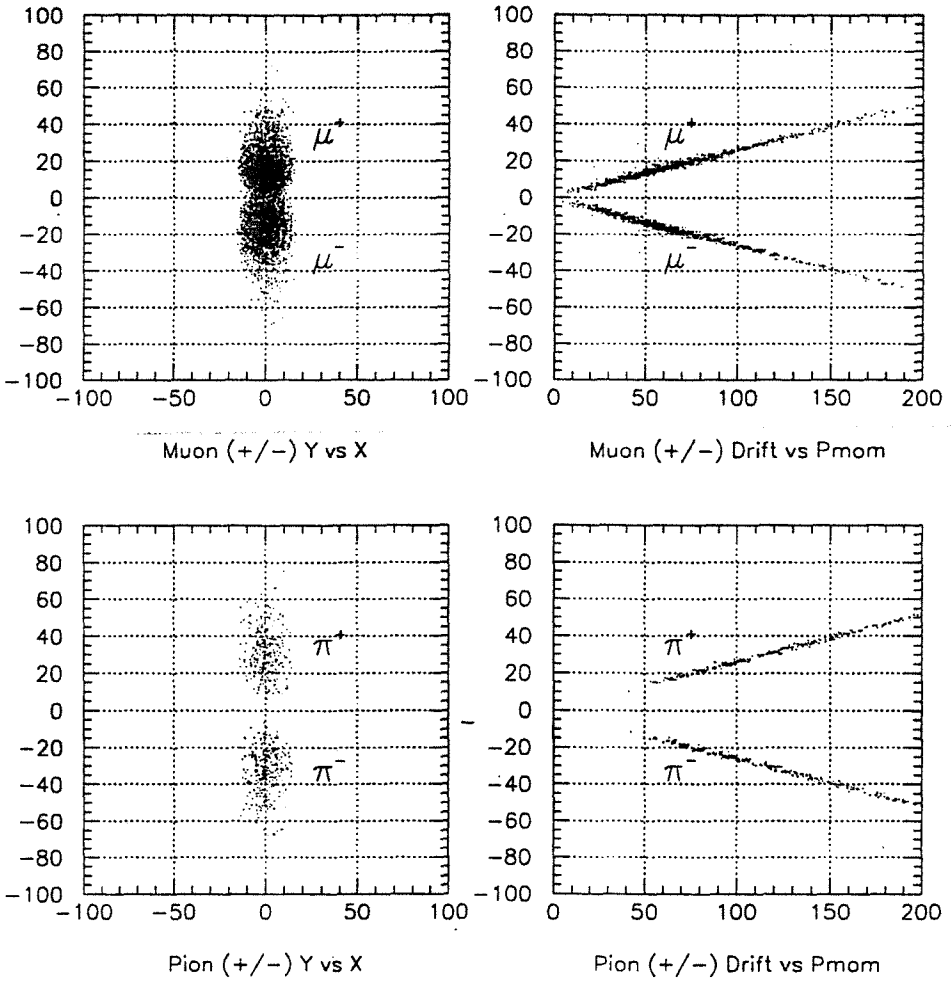

Figure 14: Scatter plot of the x-y coordinate of muon and pions in a plane of constant z in a transport solenoid after bending through $\pi/2$ and the drift distance of the centroid of the helix as a function of momentum for the same z coordinate. Results are shown for pions and muons of both charges.

fraction is 2×10^{-2}, and the conversion probability in the target with an electron having the correct energy is about 10^{-4}. Hence, we expect about 10^{-8} electrons from radiative pion capture per muon stop. Since we effectively use only 24% of the muon stops (60% convert, and 38% convert in the detection time window), we have 4×10^{-8} background electrons per effective stop. Hence, to get an expected background rate of 10^{-17} would require a ratio of protons incident during the detection time to protons incident in the main pulse of 2.5×10^{-10}. The GEANT simulations were done with a transport solenoid length of 6 m. With a 12 m transport solenoid length, the pions are attenuated due to decay by an additional factor of about .5 and hence the required attenuation is about 5×10^{-10}. We are working on means for suppressing pion transport through the channel, and are optimistic that this requirement on proton extinction can be reduced.

The background due to late arriving pions is very difficult to simulate. We make here

some general comments. First, in principle, in a transport solenoid with constantly decreasing magnetic field, there is a maximum flight time for particles with given velocity. This is a consequence of the invariant quantity p_T^2/B and conservation of kinetic energy. For given velocity, late arriving pions will be those with helical trajectories with large ratio of transverse to longitudinal momentum, so the total path length per distance along the solenoid is large. However, the longitudinal momentum will increase as the particle propagates along the solenoid. Even in the case where the momentum is initially transverse, there will be a maximum propagation time. The only caveat is that scattering in a constant field region can result in a trajectory with arbitrarily small longitudinal momentum and hence arbitrarily late arrival time. If the field is continuously decreasing, even events which scatter to purely transverse trajectories will have a limited transport time to the detection solenoid.

10 The Proposed Detector

10.1 Overview and Design Considerations

An experiment to reach the design sensitivity must achieve excellent energy resolution to eliminate intrinsic background, operate with the high stopping rates required, and eliminate other sources of background (cosmic rays, albedo from dumps, etc.).

Both SINDRUM2 and MELC use a tracking spectrometer in a solenoidal field to measure the electron energy. The SINDRUM2 detector surrounds the stopping target and achieves an electron energy resolution of about $\sigma_{RMS} = 1.0\ MeV$, limited by dispersion in energy loss in the target and detector. The proposed MELC spectrometer differs from that of SINDRUM2 in that it is displaced along the solenoid axis from the stopping target and operates in vacuum. It was technically very challenging, and for the thinnest detector envisaged had a resolution of about $\sigma_{RMS} = 0.6\ MeV$. Our goal in a detector design is an intrinsic RMS resolution of 0.25 MeV.

The SINDRUM2 experiment was run at a stopping rate such that detector rates were not a difficulty. At the higher rates we propose, it appears as if detector rates in a similar geometry would be a serious concern. By displacing the detector along the solenoid, the solid angle subtended by the detector for photons is reduced; we currently plan to use such a detector configuration.

The SINDRUM2 experiment was essentially self shielding from cosmic rays which produced photon conversions in the target, since the target was surrounded by the detector. Most cosmic ray induced events had other hits in the detector which could be used to identify and reject cosmic ray background. With the displaced detector in MELC, this feature is lost, and active as well as passive shielding will probably be required. Other CR background could be produced in other material, either in the detector elements or in the pole pieces of the magnet. By putting the stopping target in a region of the solenoid where the axial field component is decreasing linearly with position along the solenoid, all electrons with production angles between 60° and 120° (for which the proposed apparatus has good acceptance) will enter the detector region with approximately the same helical pitch, of about 50°. This is not true of electrons produced at other positions (from the entrance face of the detector solenoid, for example), and hence none of these will contribute to background unless they

subsequently scatter in the target or detectors, and the scattered trajectory is at the correct pitch and points back to the target.

We have arrived at a first pass detector which uses the MELC idea of displacing the detector from the stopping target. The implementation of tracking devices is very different. It is simpler, appears to have better intrinsic resolution, and relies mostly on proven technology.

10.2 Stopping Target Design

The stopping target should be designed to maximize stopping rate while minimizing energy loss dispersion for electrons exiting the target. The job is clearly more difficult with a broad band muon beam where one is required to stop a large momentum interval to get the required stopping rate. The transverse size is also limited by acceptance and background considerations; larger radius makes it more difficult to get large acceptance without also getting large detector rates from muon decay in orbit electrons.

The nominal target consists of 25 layers of aluminum, each 200 μm thick, with radius 7.0 cm and distance between layers 5 cm. They are positioned as shown in figure 17 in a field of 1.5 T. For the nominal beam, 24% of the muons are stopped. In figure 15 we show the dependence of the stopping rate on target radius, and also the affect of increasing the total thickness by 25%. Increasing the radius increases the rates in the detector from decay in

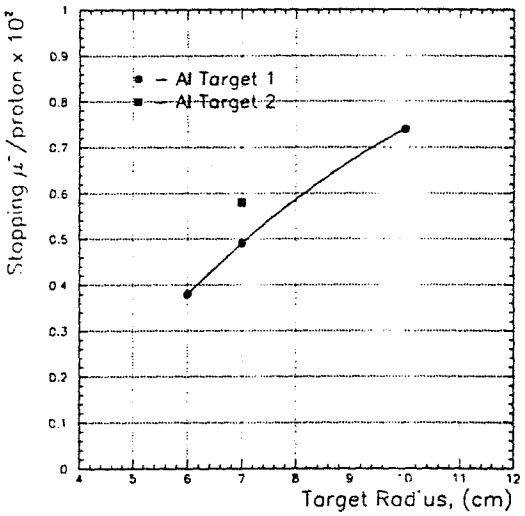

Figure 15: The dependence of the stopping rate on the target diameter and on the total thickness of the target. Target 1(2) is 25(31) layers each .02 cm thick.

orbit electrons, while increasing the total thickness increases the dispersion in energy loss in the target. Figure 16 shows the axial position where muons stop and the energy of conversion electrons downstream of the target, showing the effect of energy loss in the target.

We discuss in the next section the contribution to the electron energy measurement due to straggling in the target. We are continuing to work on optimizing the stopping rate and

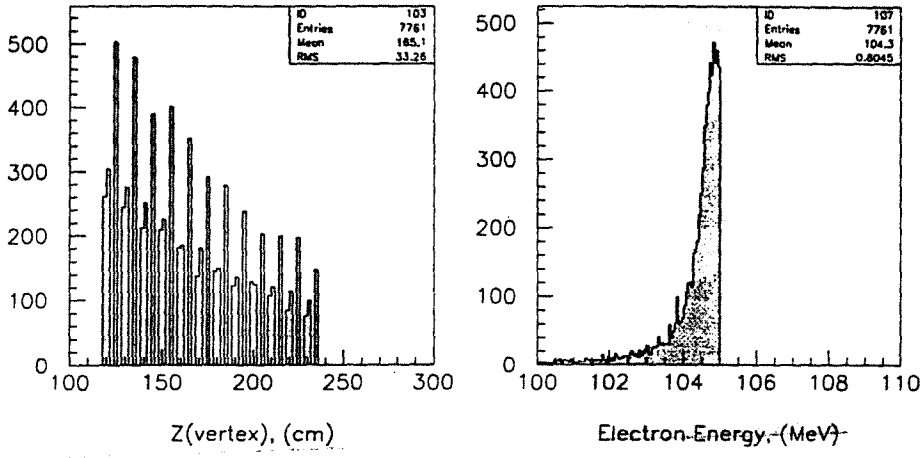

Figure 16: The axial position where muons stop (left)and the energy of conversion electrons downstream of the stopping target. Distributions are for 25 layers of $0.02cm$ aluminum target.

energy loss by varying the target, beam, and detector properties. It is a highly dimensional space in which to optimize and we are optimistic we can improve on the performance.

10.3 The Proposed Detector Solenoid and Tracking Detector

The proposed detector solenoid with tracking detector is shown in figure 17. It consists of a 6m long solenoid of radius 0.9 m. The axial component of the field varies with distance along the solenoid as shown in figure 17. The detector is in a 1T field. It consists of 5mm diameter straw tubes, arranged in a cylinder and 8 *vanes* extending radially outward from the cylinder. Each of these has 3 layers of axial straws. We assume a straw wall thickness of 25 μm of mylar or kapton. We assume the axial coordinate will be measured by capacitive coupling to foils on the outsides of the three layer array, either on only the vanes or on both the vanes and the cylinder. For multiple scattering calculations, we assume 25 μm foils on both sides of all detectors. We assume the gas manifold and straw mounting on each end of the straws can be made of beryllium with 2 gm/cm^2 thickness for axial trajectories and a width perpendicular to the straws of 2.0 cm.

The design criteria for the detector is to measure with good efficiency the parameter of the helix trajectory of electrons. Simulations show that the precision of the radius measurement is dominated by multiple scattering and is minimized by measuring one half turn of the helix. Detectors are optimally positioned at the ends of the measured trajectory and at the midpoint. The cylinder diameter is chosen to measure on average one-half helix turn. This in turn sets the maximum stopping target size for a given flux of electrons from muon decay in orbit intercepting the detector. To set the scale of the trajectories, figure 18 shows a slice of the detector at constant z, with three circular trajectories superposed. We give the transverse momenta of these trajectories referenced to the stopping target position. They are 55 MeV/c (the momentum exceeded by only 0.3% of decay in orbit electrons), 91 MeV/c (the transverse momentum of a conversion electron emitted at 60°), and 105 MeV/c. The

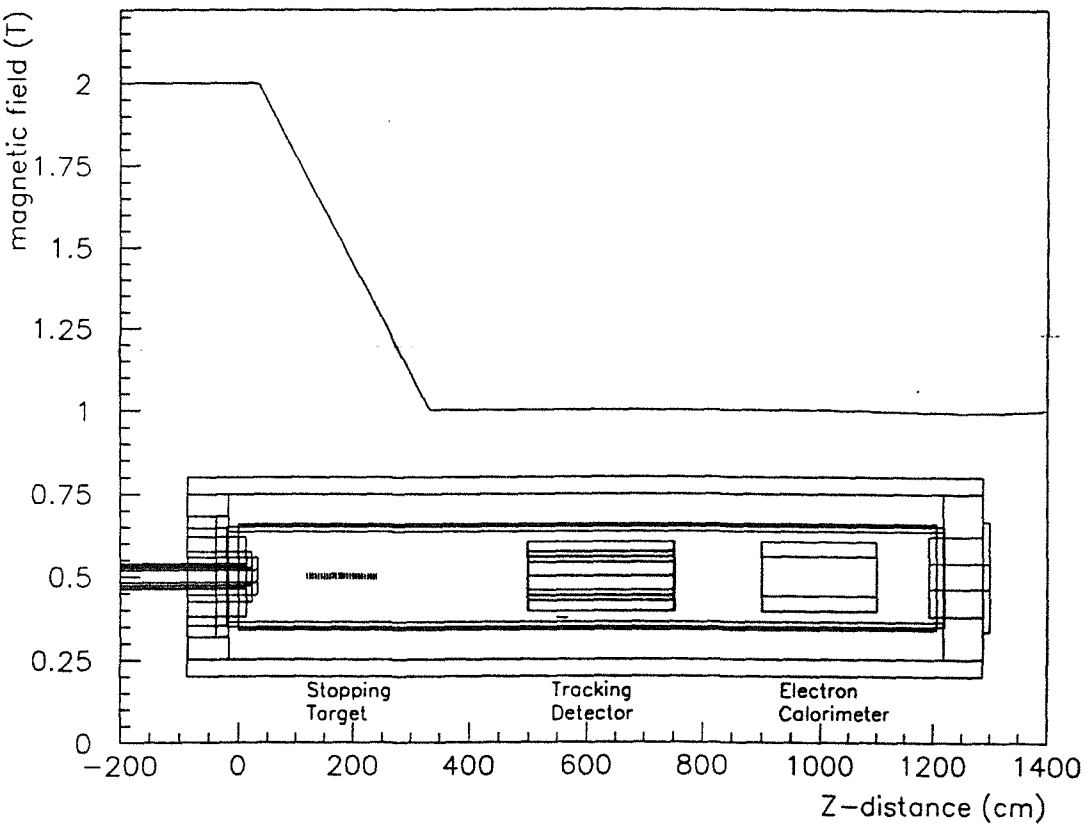

Figure 17: Schematic drawing of the detector solenoid with stopping target, tracking detector, and electron calorimeter. The drawing is superimposed on a plot of the magnitude of the axial component of the magnetic field.

cylinder radius is 38 cm, the vanes extend radially for 18 cm, and the physical target radius is 6.5 cm.

A useful relationship to recall is that the transverse momentum in an axially graded magnetic field varies, with p_T^2/B constant, and that transverse coordinates (helix radii, center position) vary, with $R^2 \times B$ constant. Hence, compared with the same quantities at the stopping target, the transverse momentum at the detector location is smaller by a factor $1./\sqrt{1.5}$ and the transverse coordinates larger by a factor $\sqrt{1.5}$.

10.3.1 Acceptance

We have estimated the acceptance using two simulation codes. The first was a simple code, working in transverse coordinates only, at the detector position. Electron starting points were distributed uniformly in a stopping target with effective radius equal to that of a physical target of radius 6.5 cm. Transverse momenta corresponding to that of electrons emitted

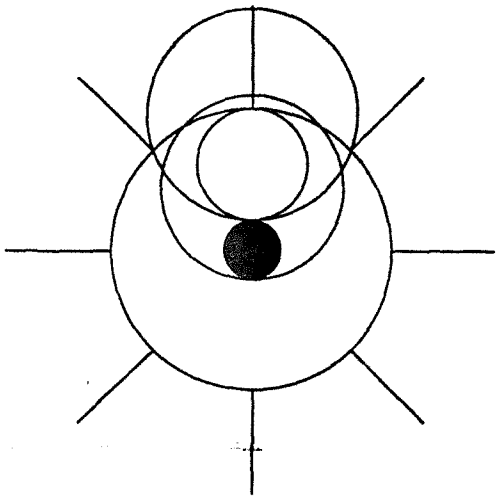

Figure 18: A cross section of the detector, effective target size, and trajectories for electrons created in the target with transverse momentum of 55, 91, and 105 MeV/c. The trajectories are shown in the region of the detector and are positioned to show the minimum allowed inner radius to keep rates from muon decay-in orbit manageable, and the detector required to have good acceptance and resolution for conversion electrons. The cylindrical part of the detector has radius 38 cm.

between 60° and 120° were generated. Electrons were allowed to scatter with RMS angle appropriate to the detectors, and hit positions were recorded for one helical pass through the detector. All such events have at least 3 layers of detectors hit, and 92% have 4 or more hits. Figure 19 shows the number of hit detectors (one hit for each pass through a vane or the cylinder) and the distribution in the value of helix angle measured in the detector. The detector has good acceptance for electrons emitted in half the solid angle, and most events have radii measured using half a helical turn. This simulation was used to get a first pass detector design.

To get a more realistic measurement of the acceptance, a full GEANT simulation of the target and detectors was done. This simulation generated the full angular distribution, and distributed starting points appropriately through the stopping target. Figure 20 shows a few typical events in the simulation. For 39% of all events, four or more detectors were hit in a single helical pass of at least 150° through the detector, and 43% had at least 3 hits. Events in which the electron passed through the gas manifold on the way in were not accepted. About half of the accepted events first hit an active element while entering the inner surface of the cylinder and about half first hit a detector either in a vane or on the outer surface of the cylinder. We tabulate the effect of all acceptance and other selection criteria in the section on estimating the sensitivity.

Figure 21 shows the z distributions of the first and last hits in the first complete helical pass through the detector (a pass entering the cylindrical detector from the inside). From these distributions, we have chosen the length of the active detector to be 2.5 m. The position of the beginning of the detector chosen to minimize the number of conversion photons, as

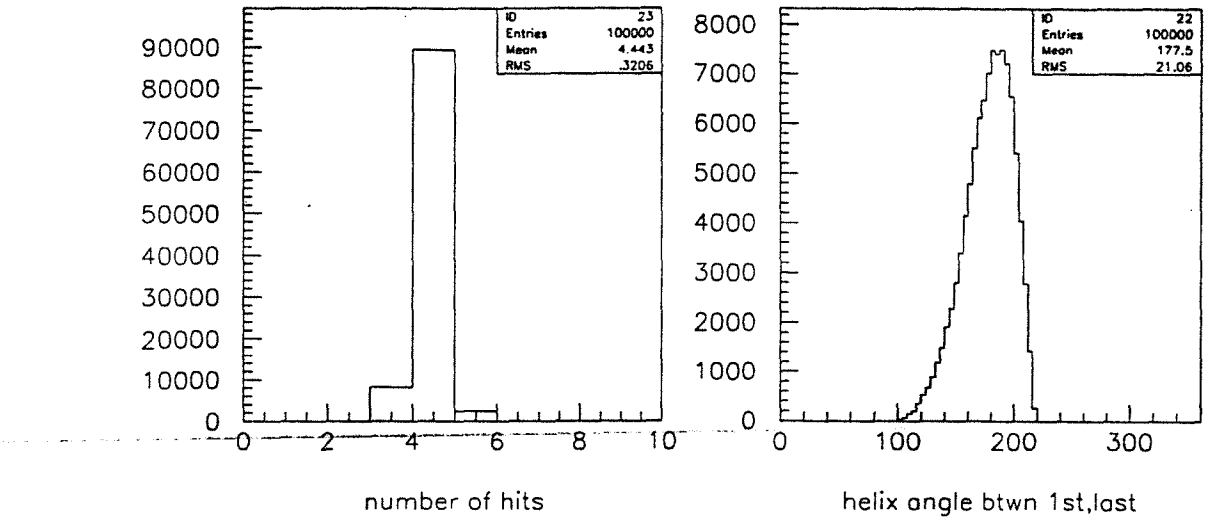

Figure 19: The number of passes through detector planes (left) and the helix angle subtended by the detector. Typically, half a turn of the helix is measured in the tracking detector with four measurements of the trajectory.

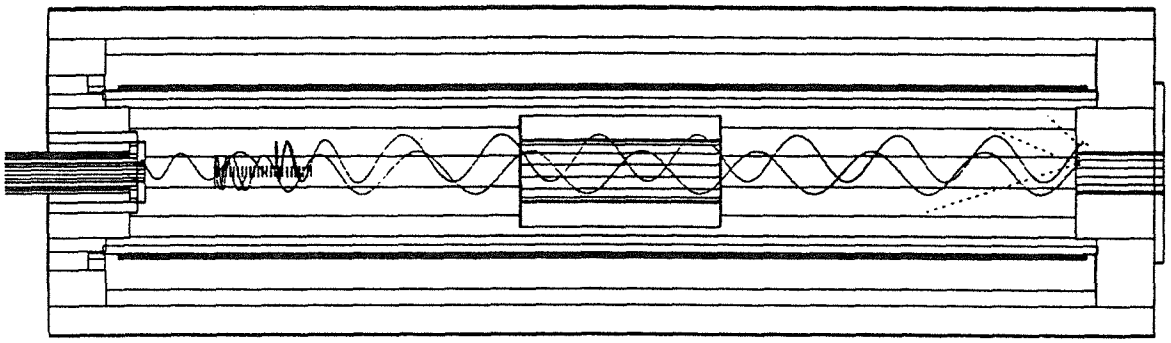

Figure 20: A few sample trajectories from the GEANT simulation.

discussed in a following section.

The optimization is undoubtedly not complete, and as we get more reliable rate calculations, we may be able to increase the target size to get more stopping rate, or decrease the inner radius to get better acceptance. These studies will be continued for the proposal.

One additional concern for the acceptance is the overlap of hits from multiple turns in the detector. Two ways exist to eliminate overlaps. One is to introduce energy loss between turns by putting material on the inner side of the solenoid. Since we measure the trajectory after passing through this material, scattering in it does not affect the energy measurement. Energy loss dispersion does affect the measurement precision, and it may not be a good idea for that reason. An additional advantage of this material is that it would absorb low energy (and high momentum) protons. A second way to eliminate overlaps is to have the

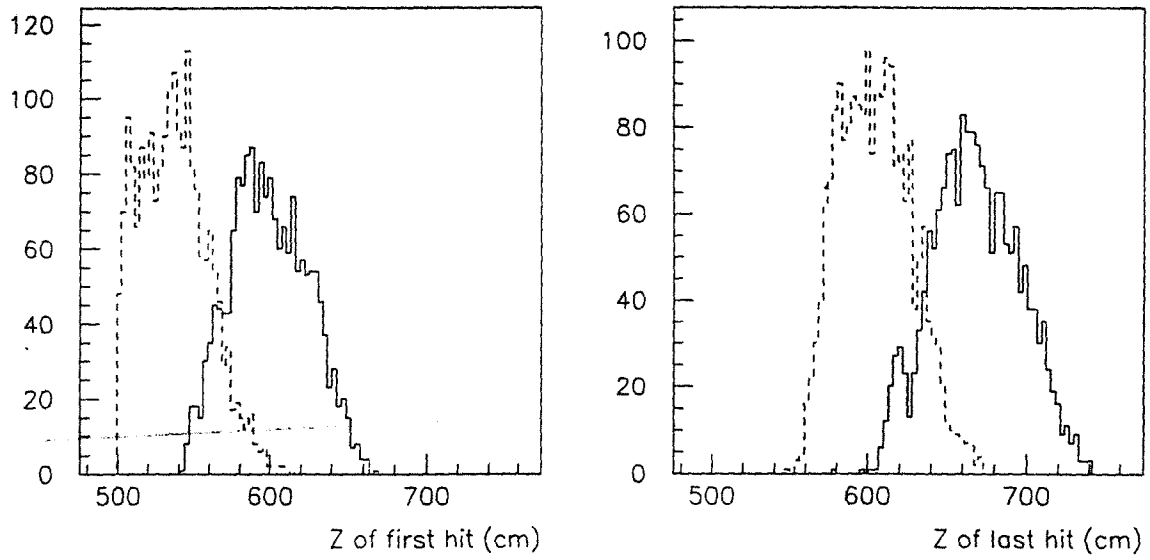

Figure 21: Distributions of the z coordinate of the first and last detector hit for the first full helical pass through the active detector. The solid(dashed) curve is for trajectories with first pass through the cylindrical part of the detector through the outer(inner) surface.

downstream end of each straw at larger radius than the upstream end, so that the second pass would hit a different straw. The radius would have to be larger by about 1cm, or 3%, introducing a 3% inefficiency per layer due to gaps (for the cylindrical detector only). We will pursue these two possibilities.

10.3.2 Resolution

Both Monte Carlo simulations were also used to estimate resolutions. For the simpler program, scattering was introduced at each layer with the appropriate σ_{RMS}. Hit positions were calculated, and the helix radii were calculated from the hit positions The fractional error in the measured radius (and hence transverse momentum) was found to have an RMS dispersion of 0.25%. By introducing energy loss with the appropriate mean value and dispersion and by introducing measurement error with σ_{RMS} of 200 μm, it was demonstrated that these cause negligible additional error in the transverse momentum measurement.

The full GEANT simulation was also used to calculate the resolution. This simulation differs from the simple program in that the full Moliere scattering formalism was used, and Landau fluctuations in the energy loss are incorporated. In addition, three dimensional trajectories are used, and both transverse and total momenta are measured. No measurement error has been introduced since this was shown to have negligible effect in the simple simulation. Figure 22 shows the distributions in the fractional energy resolution of the detector, excluding the effects of energy loss in the target, and in the total resolution, including the contribution from energy loss in the target. The fitted σ_{RMS} of the two distributions (detector resolution, total resolution) are 0.28 MeV and 0.40 MeV, where for the latter, the fit is to the data with energy above the half maximum point below the peak. The latter

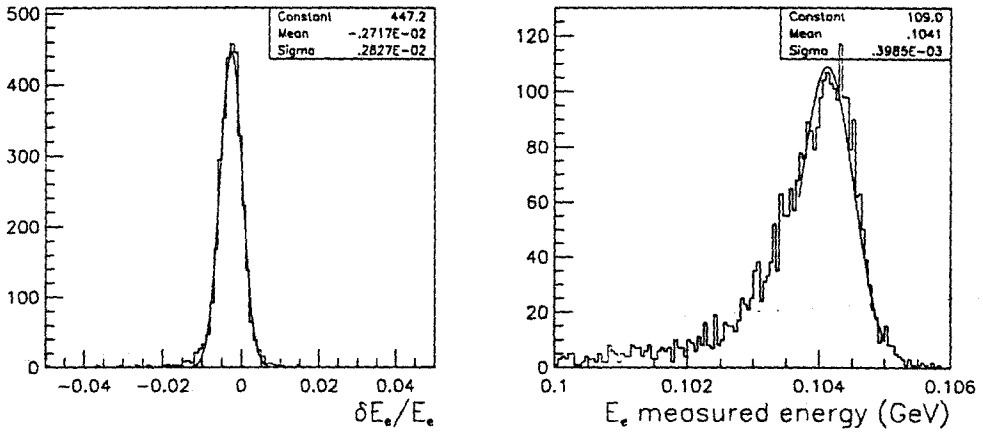

Figure 22: The distribution of the measured energy of electrons within the detector (the spectrometer resolution) and the total energy resolution.

distribution is corrected for the average energy loss in tracking detectors, different for each event but possible to know event by event by tracking back through the detectors.

The have selected events to improve measurement precision only on the basis of the number of hits and the fraction of the helix measured. We have made no attempt at a selection on the quality of the fit – since we have 4 measurements, there is one degree of freedom and can in principle select on a fit quality. We are actively working on getting the best energy measurement and getting selection criteria to eliminate events with large scatters and hence possibly poorly measured energies.

At the current state of detector design we have not reached our design goal of 0.25 MeV energy resolution. The intrinsic detector resolution is about that, but energy straggling in the target is a substantial additional contribution. We do note that the straggling contribution is very asymmetric. If we assume that electrons with energy more than 1 MeV below the peak in the measured energy distribution are lost, that effectively decreases our acceptance by about 20%. In our discussion of the expected sensitivity, we will apply a selection criteria, accepting only events with measured energy above some value.

We have not yet done a convolution of the theoretical energy distribution of decay in orbit electrons with the energy resolution function of the experiment to see the expected energy distribution of background events is. We expect it is somewhat better than that of the MELC proposal (see figure 8), given the somewhat improved energy resolution.

10.4 The Electron Calorimeter

We have done essentially no work on design of the electron calorimeter. We here only note the purpose of the device and the things which drive the design. The primary purpose is a triggering device. Backgrounds from negative muons and pions are thought to be negligible

and even a rudimentary calorimetric device should suffice for helping with that. For real electrons, it does not seem plausible to have a calorimeter which can do more than a rough check of the energy. The triggering issues are discussed in the next section. We imagine a device consisting of absorber and scintillating fiber. The light may be transported out of the solenoid to PMTs, or high field PMTs could be used. The segmentation is given by rate considerations and the potential use of spatial correlations with hits in the tracking spectrometer.

10.5 Triggering and Data Acquisition

We have done essentially no design of the triggering and data acquisition. The channel count is modest, probably under 20000 channels of either time or pulse height.

The signals available to a trigger are the electron calorimeter signal and fast outputs from the tracking devices. One can imagine a trigger consisting of localized energy in the calorimeter, and sets of hits in the tracking chambers in close proximity – for example requiring four groups of at least two adjacent straws hit, with two groups in the cylinder and one group in each of two vanes with azimuthal angle between those of the groups in the cylinders. The calorimeter signal may also be put in spatial coincidence with the tracking signals.

We envisage a data sparsing readout. One similar to the E791/E871 drift and straw chamber readout would probably have the requisite bandwidth. The calorimeter readout would preferably be a flashencoding ADC. Since there is a time structure of 1 MHz, it is unlikely that we would be reading out more than one event per pulse. It may also be advantageous to record the signals in some fraction of the detectors during the full 500 or so ns of the detection time for the muon pulse in which the event is detected.

We anticipate that on the time scale of the proposal we will have a much better idea of expected trigger rates with a sensible trigger and data acquisition scheme.

10.6 Rate Estimates

Rates in the detector derive from a number of sources. They can be divided into prompt (those occurring during the time when the muons are brought to rest in the target) and delayed (those which occur in time with the detection of conversion electrons.

Prompt processes include scattering of primary beam particles into the detector, muon decay in flight, albedo from the beam dump, and particles resulting from pion capture. We have not done a careful simulation of these rates. If we stop 24% of muons, then the other 80% will decay with probability about 1.5hit in the detector is higher than for a stopped muon because the distribution of the decay point extends to larger radii. The resulting rate could be equal to or larger than that for stopped muons. Similarly, there are potentially large rates from pion capture and from scattered particles, which we must understand. We note that it should be possible to reduce the gain in the detectors substantially during the stopping pulse so as to prevent excessive currents in chambers and reduce aging effects. Both the expected rates and means to protect the detectors must be studied.

We have better estimates of the rates in detectors during the detection time. We include here estimates of rates from the following processes:

- Electrons from muon decay in orbit
- protons from nuclear deexcitation following muon capture
- photons from nuclear deexcitation following muon capture

10.6.1 Rates from muon decay in orbit

The energy distribution of electrons from muon decay in orbit has been calculated in reference [16]. They tabulate their result for different elements; magnesium is the closest to aluminum. The distribution in energy, and the integral distribution above any energy is shown in figure 9. We have estimated the rate from this source by generating electrons with energy above 51.1 MeV (4.9% of all decay electrons) according to this distribution, and distributed uniformly in the target and in solid angle. The probability of intercepting the detector was calculated to be .023%. The instantaneous rate is then estimated by assuming an average stopping rate of 10^{11}, a decay probability of 0.5, probability of decay in the detection time of 0.38, a macro duty factor of 50%, a micro duty factor of 50%, and assuming each electron hitting the detector will hit 20 straws (since the trajectory is close to tangent to the cylindrical part of the detector). This results in a rate of $.049 \times .00023 \times 10^{11} \times 0.5 \times 0.38/0.5/0.5 \times 20 = 18MHz$. Most of these hits are in the cylindrical part of the detector, which contains about 1400 straws. The individual instantaneous rate is then under 13 kHz.

10.6.2 Albedo from pole pieces

A fraction of the muon decay electrons will hit the pole pieces of the detector solenoid and emit low energy photons and electrons which can traverse the detector. Also, some muons will stop in the pole pieces and their decay electrons can cause hits in the detectors. We will study these processes with our full GEANT simulation. By careful design of the pole pieces so that particles are dumped near the axis of the solenoid, it should be possible to reduce the probability of albedo hitting the detectors.

10.6.3 Photons from radiative muon capture

Approximately 2 photons are emitted for every muon capture. Since roughly equal numbers of muons are captured as decay, the factors for duty factor, capture probability, capture in the detection time are the same as in the previous case. Hence, we expect an instantaneous flux of about 1.5×10^{11} photons per second to be emitted isotropically from the stopping target. Conversions will occur in the endplates of the active detectors and in the straws themselves. The photons are typically a few (up to 10) MeV. The detector endplates each subtend about 0.2% of the solid angle. Assuming a typical path length in the endplate of 2 gm/cm^2 of carbon (for which scattering cross sections are easily available), the conversion probability for a 10 MeV photon is about 0.01. Hence, the instantaneous conversion rate is about $2 \times 10^6\ s^{-1}$. The conversion electrons will typically spiral for a few tens of ns and hit 10 tubes. The rate per tube is then about $10^4 s^{-1}$ for conversions in each endplate, assuming every conversion gives an electron moving into the active region. Conversions in the straws

are about equal to the sum of the two endplates, giving a total instantaneous rate of about $4 \times 10^4\ s^{-1}$.

10.6.4 Protons from muon capture

Approximately 1% of muon capture events result in a proton being emitted from the nucleus. The protons have low kinetic energy, but rather high momentum. If we assume all these protons intercept the detector and result in 20 hits per proton, the average rate in a straw during the detection time is close to 10 MHz. Hence, a reduction of about a factor of 100 is required. In fact, some of these protons are absorbed in the stopping target, and others can be absorbed in a thin absorber of cylindrical shape between the target and detector; its radius can be chosen to have no effect on conversion electrons. We have estimated that these two mechanisms reduce the flux by about a factor of 3 with no loss in electron detection efficiency.

We have studied ways to further absorb protons, for example by exploiting the fact that their helical trajectory has the opposite screw sense of that of electrons. One idea is to use a set of baffles in the shape of turbine blades (see figure 23).

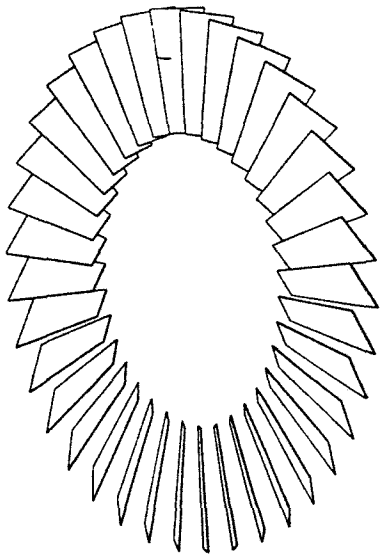

Figure 23: Drawing of a baffle to preferentially attenuate positive particles traversing the region between the stopping target and the tracking detectors.

Electrons with 105 MeV mostly pass parallel to the blades, and hence have a low probability of hitting them. Protons pass perpendicular to the blades and are substantially absorbed. A factor of 100 suppression has been achieved with 5 baffles between the target and detector, with a loss of less than half the electrons. Very low energy protons may also be preferentially absorbed by a low Z absorber of modest thickness on the interior of the cylindrical straw array and on the entrance face. That is also discussed in the context of slightly changing the radius of curvature of electrons in their second pass through the detector, to avoid getting overlapping trajectories. We have not yet optimized such a device and determined if it would unacceptably worsen the resolution.

We will continue these studies and are optimistic that we can improve on the ratio of proton absorption to electron loss.

11 Expected Sensitivity

We define an accepted event to be one in which we have at least four hit detectors in a single helical pass through the detector, for which the electron did not hit the upstream gas manifold, and for which the measured electron energy exceeds 105 MeV. Table 3 shows the number of muon stops in an exposure of 10^7 seconds and the sequential affects of factors which affect the sensitivity.

Running time (sec)	10^7
Proton flux (sec^{-1})	2×10^{13}
μ/p entering solenoid	0.020
Stopping probability	0.24
Fraction of μ which capture	0.60
Fraction of μ which capture in time window	0.38
Fraction of electrons entering detector volume	0.72
Fraction of electrons missing gas manifold	0.81
Fraction of electrons with $\Delta\phi > 150°$	.66
Fraction of electrons with at least 4 hits	.89
Fraction with E_e within 1 MeV of peak	.80
Total/$R_{\mu e}$	6.0×10^{16}

Table 3: A summary of the expected sensitivity for a one year (10^7 s) run, showing the loss of sensitivity due to various factors. The expected sensitivity is increased by a factor of 2.2 if a mercury rather than a copper target is used, and decreased by a factor of 2 if we use a turbine shaped baffle to attenuate by a factor of 100 the flux of protons hitting the detector.

The numbers for the muon flux and stopping probability are calculated as discussed in the preceding text. The ratio of capture rate to decay rate is 1.52. We assume a time between muon pulses of 890 ns, and that we are sensitive for the second half of that time to get the fraction which capture in the sensitive time. If we capture for only 360 ns beginning 530 ns after the proton pulse, the number of expected events would be .76 times what is quoted. The factors for acceptance (entering the detector, missing the manifold, and electron energy in the main peak) are calculated in the full GEANT simulation of the detector. Using a mercury rather than copper target results in a factor of 2.2 higher muon stopping rate. Using a turbine shaped baffle to attenuate by a factor of 100 the flux of protons hitting the detector causes a loss in sensitivity of about a factor of two.

What is not included in the expected sensitivity is all the difficult things to calculate: trigger efficiencies, deadtimes, other analysis losses, etc. At this point we do not attempt to estimate these factors.

12 Manpower Issues

For a number of years, this experiment has been without a plausible place at which it could be mounted. That has resulted in a lack of serious effort on designing a beamline and experiment. When the possibility of mounting an experiment at BNL was realised, interest in forming a collaboration increased. This letter is signed by groups from five institutions. In addition, Bill Morse (BNL), Dan Marlow (Princeton), and Steve Schnetzer (Rutgers) are interested in participating but have chosen not to make a commitment at this time by signing this LOI. We expect that a group of at least 50 physicists with substantial support from the laboratory will be required to execute the experiment. We are actively working to strengthen the collaboration and anticipate this will be easier as it becomes more clear that BNL will be a viable place to do experiments in the next five years.

The potential contributions from the INR group is important. That group is responsible for many of the critical ideas for the experiment. There is the possibility that they could contribute substantially in the way of material for the beamline and solenoids. At issue is the mechanism for them receiving support for their participation, given the financial support for research in Russia at the present time.

We intend that by the time of the proposal there will be more names associated with each institution, that there will be a BNL participation in the collaboration, and that we will add a few more institutions.

13 Schedule for Producing a Proposal

Our intention is to produce a full proposal in the next 6-8 months. The work during that time will encompass the following:

- tests of mechanisms for bunched beam extraction and measurements of the extinction that can be achieved in the two schemes presently envisaged.
- design of a secondary extinction scheme for the proton beam, and possibly a means of providing extinction in the muon beam itself.
- studies of the time structure in the muon beam.
- optimization of the muon source to maximize flux.
- work on mechanisms for further purifying the muon beam and sign selecting the beam.
- optimization of the detector geometry, stopping target, and beam line to maximize sensitivity and minimize backgrounds.
- further studies of the expected rates in the detector.
- studies of the ability to reconstruct electron trajectories in a realistic detector environment and how the resolution improved.
- initial design of the proton beam, target, solenoids, and beam dump.

- conceptual design and possible prototype of the tracking detectors.
- conceptual design of the electron calorimeter.
- design of triggering and data acquisition schemes.
- realistic costing of the beam elements and the detectors.

We anticipate that by the time of the proposal we will have substantially strengthened the collaboration and will have assigned responsibility for major parts of the design and construction.

14 Costs and Resources

While all of the components of the beamline and detectors seem fairly conventional, we have had neither the time nor the technical resources to do the costing. We here make some general comments.

It appears as if the cost will be dominated by that of the solenoids. Based on the stored energy in these devices and the cost scaling from reference [21], a naive estimate for these devices is \$11.1M. For purposes of this estimate, we have taken the production, transport, and detector solenoids to have the dimensions in shown in table 4, which also shows the cost.

Solenoid	Field(T)	Radius(m)	Length(m)	Energy(MJ)	Cost(M\$)
Production	3.5	0.6	4.0	22.1	4.1
Transport	2	0.5	12.0	15.1	3.1
Detector	1.2	0.9	11.0	20.6	3.9

Table 4: Size and approximate cost estimates for the three solenoid systems in the experiment.

In the table, we have assumed the sizes of these devices will be at the upper end of the range of possible sizes. The costs do not include return yoke or refrigeration. Mike Green, one of the authors of reference [21], has told us that the parameters of the magnets are sufficiently standard that one can use the scaling law, recognizing that the data used to predict this law show a substantial scatter. He estimates the refrigeration at below 1 kW, and hence a relatively small fraction of the cost. The need for a full flux return is unclear; it will probably be needed at least for the downstream end of the detector solenoid, where field quality is important, and for the transition regions between solenoids.

The production solenoid will have some complications: radiation and heat shielding, entrance and exit ports for the proton beam, and coupling to the transport solenoid. The transport solenoid is relatively conventional; the only complications are the curvature, the necessity for installing absorbers, and the coupling to the other solenoids. The detector solenoid is similarly straightforward. Careful attention to the coupling of all solenoids will be required to ensure that the axial component of the field is continuously decreasing and hence eliminate reflections.

There do exist a number of solenoids, and it is possible that one or more of them could be used for the experiment. We will explore the possibility of using them when we have a better idea of the required properties of the solenoids.

A second issue which we can explore when the experiment is on slightly firmer footing is the possibility of getting some resources from INR Moscow. For example, they have a substantial fraction of the steel that would be required for the magnet return yokes. That also have appropriate aluminum for the vacuum vessels and superconducting cable which could in principle be used for the lower field solenoids.

The tracking detectors appear to be rather conventional, assuming that the idea of using straws works. Two complications are the need to get measurements of the axial coordinate and the need to operate in vacuum. The number of channels is modest, under 3000 straws and under 10000 pads to measure the axial coordinate. if it can be done that way. We have done even less work on the electron calorimeter, and hence have no cost estimate. However, the volume is rather small, the required resolution is not excessive, and we don't expect this to be a substantial fraction of the cost. An active anticounter surrounding the detector will likely be required to eliminate cosmic ray background. An area of under 100 m^2 of scintillator will be required. Electronics will be required for about 20000 channels of straw tubes and cathode pads, calorimeter segments, and veto counter channels. They will require either time or pulseheight, and in some cases both.

We have not yet looked seriously at operating costs. Most of the magnetic volume is superconducting, and hence not a large power user. If the idea of the muon collider group of using a copper insert in a superconducting solenoid to increase the field (and provide heat and radiation shielding) is used, that could be a relatively high power device, but would probably reduce the capital cost. A second possibly high power device is the pulsed kicker magnet for the secondary extinction device. We have estimated that the power needed to cycle a device with suitable magnetic field and volume is on the order of 1 MW delivered to the magnet, assuming none of the energy in the field is recycled. The power supply must operate at 1 MHz.

If we run at 8 GeV in the AGS, the operating cost of the AGS will also be rather modest. Since it is unlikely that other experiments will be able to run simultaneously, only one beam line will be powered. We have asked the laboratory to estimate the running costs for 8, 14, and 24 GeV with a duty factor of 0.5.

15 Requests of the Laboratory

There are a number of areas in the design of this experiment for which we have neither expertise nor the resources to hire such expertise. These are mostly in the beam line devices: a rapid cycling fast kicker magnet, the primary proton transport in general, the muon production target, and the various superconducting solenoids. A design sufficient to do a cost estimate for construction will be very important on the time scale of a full proposal. We request from the lab the resources to begin the design of these devices, which are critical to the success of the experiment. We anticipate that members of the collaboration could interact rather closely with engineers and physicists at BNL in that design work. If the appropriate personnel are not available at BNL, then we would like the assistance of the lab

in finding and supporting design work by personnel from national labs or other sources.

In the next fixed target running period, we would like to test the bunched beam extraction schemes. We have done preliminary tests of a bunched beam extraction using the AGS RF structure. That frequency is not ideal for our purposes, and we would like to consider how we could get a better bunch spacing. The barrier bunch extraction scheme has not been tested, and we request that the RF cavities needed to test that be installed and the tests done in the next year.

16 Summary

We are enthusiastic about the possibility of doing a muon to electron conversion experiment at the AGS. The physics motivation is extremely strong. Independent of theoretical considerations, pushing a test of a fundamental symmetry by a factor of $10^3 - 10^4$ is clearly valuable. In addition, ideas based on grand unified supersymmetric models make plausible the possibility of discovering lepton flavor violation in the range of sensitivity of the proposed experiment.

The BNL AGS is uniquely suited to provide the muon beam required to do this experiment. For a variety of reasons discussed above, the experiment cannot be done at the low energy facilities (PSI, TRIUMF, LANL, MMF) where these kinds of experiments have been done. The AGS proton energy allows a significantly higher flux muon beam to be made. Possibilities exist for making an appropriately pulsed beam, and these ideas can be tested in the next few months.

Preliminary studies of physics backgrounds and detector rates are promising. There are many things which remain to be optimized before a compelling case can be made that the experiment can reach the desired sensitivity and be background free. We are actively working on the calculations necessary for the optimization. We are requesting the laboratory's help in some aspects of the preparation of the proposal.

We intend to produce a proposal to do this experiment at BNL. The proposal will make the compelling case for the feasibility of the experiment and will be submitted by a significantly augmented group of proponents which is capable of executing the experiment. It will contain a detector and beam design sufficient for costing and demonstrating the performance of the experiment.

References

[1] R.N. Cahn and H. Harari, Nucl. Phys. B176, 135 (1980).

[2] R. Barbieri, L. Hall and A. Strumia, "Violations of Lepton Flavour and CP in Supersymmetric Unified Theories", IFUP-TH 72/94, (1995).

[3] N. Arkani-Hamed, H. Cheng and L. Hall, "Flavor Mixing Signals for Realistic Supersymmetric Unification", LBL-37343, (1996).

[4] R. Barbieri and L. Hall, "A Grand Unified Supersymmetric Theory of Flavor", LBL-38381, (1996).

[5] A. Hisano, T. Moroi, K. Tobe and M. Yamaguchi. "Exact Event Rates of Lepton Flavor Violating Processes in Supersymmetric SU(5) Model", LBL-38653, (1996).

[6] Y. Kuno, A. Maki and Y. Okada, "Background Suppression for $\mu \rightarrow e\gamma$ with Polarized Muons" LANL hep-ph/9609307, (1996).
Y. Kuno and Y. Okada, "$\mu \rightarrow e\gamma$ Search with Polarized Muons", LANL hep-ph 9604296 (1996).

[7] R.M. Djilkibaev and V.M. Lobashev, Sov. J. Nucl. Phys. 49(2), 384 (1989).

[8] "MELC Experiment to Search for the $\mu^- A \rightarrow e^- A$ Process", V.S. Abadjev, et al., INR preprint 786/92, November 1992.
R.M. Djilkibaev and V.M. Lobashev, "Beam Dynamics and Technology Issues for $\mu^+\mu^-$ Colliders", J. Gallardo ed. (1995).

[9] W.J. Marciano and A.I. Sanda, Phys. Rev. Lett. 38, 1512 (1977).

[10] J.D. Vergados, Phys. Rep. 133, 1 (1986).

[11] W. Marciano, private communication.

[12] A. vanderSchaaf, seminar at AGS2000 workshop, BNL, May 1996.

[13] S. Ahmad et al., Phys. Rev. D38, 2102 (1988).

[14] C. Dohmen et al., Phys. Lett. B317, 631 (1993).

[15] O. Shankar, Phys. Rev. D25, 1847 (1982).

[16] F. Herzog and K. Alder, Helv. Phys. Acta 53, 53 (1980).

[17] "$\mu^+\mu^-$ Collider a Feasibility Study", the $\mu^+\mu^-$ collaboration, (1996).
"Beam Dynamics and Technology Issues for $\mu^+\mu^-$ Colliders", J. Gallardo ed., (1995).

[18] H.C. Fesefeldt "Simulation of Hadronic Showeres. Physics and Applications. Report PITHIA 85-02, Achen, 1985.

[19] P.A. Aarnio, J. Lindgren, J. Ranft, et al., CERN/TIS-RP/190, (1987).

[20] V.S. Barashenkov, N.M. Sobolevsky and V.D. Toneev, Atomn. Energ. 32, (1972).

[21] M.A. Green, R.A. Byrns and S.J. St. Lorant, Advances in Cryogenic Engineering 37, Plenum Press, New York (1992).